RESEARCH ARTICLE

Plasmaspheric Hiss: Coherent and Intense

Bruce T. Tsurutani[1] (iD)**, Sang A. Park[1], Barbara J. Falkowski[1,2], Gurbax S. Lakhina[3]** (iD)**, Jolene S. Pickett[4]** (iD)**, Jacob Bortnik[5]** (iD)**, George Hospodarsky[4], Ondrej Santolik[6,7]** (iD)**, Michel Parrot[8]** (iD)**, Pierre Henri[8]** (iD)**, and Rajkumar Hajra[8]** (iD)

[1]Jet Propulsion Laboratory, California Institute of Technology, Pasadena, CA, USA, [2]Glendale Community College, Glendale, CA, USA, [3]Indian Institute of Geomagnetism, Navi Mumbai, India, [4]Department of Physics, University of Iowa, Iowa City, IA, USA, [5]Department of Atmospheric Sciences, University of California, Los Angeles, CA, USA, [6]Czech Academy of Sciences, Prague, Czech Republic, [7]Charles University, Prague, Czech Republic, [8]LPC2E, CNRS, Orléans, France

Abstract Intense ~300-Hz to 1.0-kHz plasmaspheric hiss was studied using Polar plasma wave data. It is found that the waves are coherent in all local time sectors with the wave coherency occurring in approximately three- to five-wave cycle packets. The plasmaspheric hiss in the dawn and local noon time sector are found to be substorm (AE*) and storm (SYM-H*) dependent. The local noon sector is also solar wind pressure dependent. It is suggested that coherent chorus monochromatic subelements enter the plasmasphere (as previously suggested by ray tracing models) to explain these plasmaspheric hiss features. The presence of intense, coherent plasmaspheric hiss in the local dusk and local midnight time sectors is surprising and more difficult to explain. For the dusk sector waves, either local in situ plasmaspheric wave generation or propagation from the dayside plasmasphere is possible. There is little evidence to support substorm generation of the midnight sector plasmaspheric hiss found in this study. One possible explanation is propagation from the local noon sector. The combination of high wave intensity and coherency at all local times strengthens the suggestion that the electron slot is formed during substorm intervals instead of during geomagnetic quiet (by incoherent waves). Plasmaspheric hiss is found to propagate at all angles relative to the ambient magnetic field, θ_{kB}. Circular, elliptical, and linear polarized plasmaspheric hiss have been detected. No obvious, strong relationship between the wave polarization and θ_{kB} was found. This information of hiss properties should be useful in modeling wave-particle interactions within the plasmasphere.

Plain Language Summary Plasmaspheric hiss is found to be coherent (at all local times). The coherency occurs in packets of ~3 to 5 cycles. For the dawn and noon local time sectors, a scenario of substorm and solar wind pressure generation of outer zone chorus with further propagation into the plasmasphere is supported by the data analysis results. The predominant wave polarization of hiss is found to be elliptical, with some minor presence of circular and linear polarizations. This is in general agreement with theoretical expectations.The presence of intense, coherent plasmaspheric hiss strongly supports the new hypothesis that the electron slot is formed during substorms rather than geomagnetic quiet periods. The loss of relativistic E ~ 1MeV electrons for the inner magnetosphere (L > 6) may be due to wave-particle interactions with coherent plasmaspheric hiss.

1. Introduction

Plasmaspheric hiss is a whistler mode wave with a frequency range between ~20 Hz and ~2.0 kHz, observed by satellites inside the plasmasphere (Agapitov et al., 2013, 2014: L. Chen et al., 2014; Cornilleau-Wehrlin et al., 1978, 1993; Delport et al., 2012; Falkowski et al., 2017; Gail & Inan, 1990; Gail et al., 1990; Gao et al., 2015; Glauert et al., 2014; Green et al., 2005; Golden et al., 2012; Hayakawa & Sazhin, 1992; Kim et al., 2015; Korth et al., 1986; Li et al., 2013, 2014, 2017; Li, Chen, et al., 2015; Li, Ma, et al., 2015; Liu et al., 2017; Malaspina et al., 2016, 2017; Meredith et al., 2004, 2006, 2007, 2018; Orlova et al., 2014; Santolik et al., 2001, 2006; Shinbori et al., 2003; Smith et al., 1974; Solomon et al., 1988; Spasojevic et al., 2015; Storey et al., 1991; Summers et al., 2014; Su et al., 2015; Thorne et al., 1973, 1974; Tsurutani et al., 1975, 2012, 2015; Yu et al., 2017). Thorne et al. (1973) named the waves *hiss* for the sound it made when played through a loudspeaker.

Plasmaspheric hiss has been observed during geomagnetic quiet (Carpenter, 1978; Thorne et al., 1977), during substorms (Agapitov et al., 2014; Kim et al., 2015; Li, Chen, et al., 2015; Li, Ma, et al., 2015; Malaspina

et al., 2016, 2017; Meredith et al., 2004, 2018; Spasojevic et al., 2015; Thorne et al., 1973; Tsurutani, Falkowski, et al., 2011; Tsurutani et al., 2012, 2015; Yu et al., 2017), and during magnetic storms (Bortnik et al., 2008; Bortnik, Li, et al., 2009; Bortnik, Thorne, et al., 2009; Kim et al., 2015; Smith et al., 1974; Tsurutani et al., 1975). The electromagnetic waves have been observed at all local times, with statistically more intense events observed on the dayside (Falkowski et al., 2017; Kim et al., 2015; Li, Ma, et al., 2015; Malaspina et al., 2016, 2017; Meredith et al., 2004, 2018; Spasojevic et al., 2015; Tsurutani et al., 2015; Yu et al., 2017) than on the nightside. A hiss-like emission has also been detected in high-density plasma regions outside of the plasmasphere, that is, in plasma *tails* (A. J. Chen & Grebowsky, 1974; Falkowski et al., 2017; Tsurutani et al., 2015).

Thorne et al. (1979) suggested a local generation of plasmaspheric hiss, with the waves circulating many times through an equatorial amplification region. This possible mechanism has not been ruled out. It has recently been shown that plasmaspheric hiss is most often present in the dusk sector of the plasmasphere (Tsurutani et al., 2015), indicating that ~10–100-keV electrons drifting into the plasmaspheric bulge may be a source of the waves via a local generation mechanism similar to the Thorne et al. (1979) concept.

Meredith et al. (2004) in a seminal result showed that plasmaspheric hiss was most intense in the dayside sector of the plasmasphere. More recently, Meredith et al. (2018) studying all local times of plasmaspheric hiss has found that hiss is most intense on the dayside and increases with increasing geomagnetic activity (AE) from midnight through dawn to dusk. The authors mention that plasmaspheric hiss is most intense and spatially extended in the ~200–500-Hz frequency band during active conditions. They also found that the average plasmaspheric hiss intensity in this frequency range in the prenoon sector exhibited two peaks, one near the magnetic equator and one at high latitudes. They also found that in the premidnight sector, the intensity of plasmaspheric hiss decreased with increasing geomagnetic activity.

Falkowski et al. (2017) studying dayside sector plasmaspheric hiss found that the waves were associated with both substorms and solar wind pressure pulses (for solar wind pressure effects, see also Gail & Inan, 1990; Kokubun, 1983; Shinbori et al., 2003; Tsurutani et al., 2015, 2016; Remya et al., 2015; Yue et al., 2017). The substorm-dependent scenario is that substorm-injected electrons gradient drift from their midnight sector injection to the dayside magnetosphere, generate chorus there (Meredith et al., 2001; Tsurutani & Smith, 1974, 1977), and the waves then propagate into the plasmasphere (Bortnik et al., 2008; Bortnik, Li, et al., 2009; Bortnik, Thorne, et al., 2009; Breneman et al., 2009; L. Chen et al., 2012; Li et al., 2013; Li, Chen, et al., 2015; Santolik, 2008; Santolik & Chum, 2009; Thorne et al., 1973, 1974; Tsurutani et al., 2012). Parrot et al. (2004) have shown that chorus waves could, through magnetospheric reflection, propagate into the plasmasphere (Bortnik et al., 2008; Bortnik, Li, et al., 2009; Bortnik, Thorne, et al., 2009; Parrot et al., 2004; Wang et al., 2011).

For the geomagnetic quiet events, the Falkowski et al. (2017) hypothesis is that solar wind pressure variations generate chorus in the dayside minimum B pockets via compression of remnant ~10–100-keV electrons. Their scenario is again that chorus propagates into the plasmasphere at low altitude regions of the plasmapause.

Tsurutani et al. (2015) and Falkowski et al. (2017) demonstrated that some dayside plasmaspheric hiss were coherent. This is an extremely important feature of plasmaspheric hiss because wave-particle interactions can be three orders of magnitude more intense than for incoherent waves (Bellan, 2013; Lakhina et al., 2010). This present work is intended to give a more complete, global picture of Polar plasmaspheric hiss. This study will cover the most intense plasmaspheric hiss frequency range of ~300 Hz to ~1.0 kHz. Low frequency plasmaspheric hiss, less than ~200-Hz waves (Artemyev et al., 2013; L. Chen et al., 2014; Gao et al., 2015; Li, Ma, et al., 2015; Malaspina et al., 2017; Meredith et al., 2018), will be specifically excluded because it is believed to have a different generation source than higher frequency plasmaspheric hiss.

To characterize plasmaspheric hiss at all local times, we will focus on the 10 most intense Polar wave events separately in each of the four magnetic local time (MLT) sectors: midnight (21 < MLT < 03), dawn (03 < MLT < 09), noon (09 < MLT < 15), and dusk (15 < MLT < 21). There is no overlap between the events, and they are all statistically independent. From these 40 events, we will identify the spatial location of the events, the wave coherency, and directions of propagation as well as the AE* and SYM-H* dependences (the * designates incorporation of gradient-drift time delays of ~25-keV electrons: this delay is ~1 hr to drift from midnight to noon). The instantaneous solar wind ram pressure effects will also be studied. The wave polarization (circular, elliptical, and linear) as a function of spatial location will be studied to obtain further information on the wave sources.

2. Method of Data Analyses

In this study we consider plasmaspheric hiss in the frequency range from ~300 Hz to ~1.0 kHz using ~1 year (April 1996 to April 1997) of Polar satellite data. This frequency band was found by Falkowski et al. (2017) to be the most intense plasmaspheric hiss band (see also Meredith et al., 2018), and we thus limit our present study to this region. We purposely have not considered low frequency (LF) plasmaspheric hiss which may have different distributions and sources of generation. The data can be obtained from http://cdaweb.gsfc.nasa.gov, NASA's CDAW website.

The plasmasphere was identified (Falkowski et al., 2017) using the electron plasma frequency characteristics in wave data summary plots (Santolik et al., 2001). The statistical portion of our study covers the region $L = 2$ to $L = 13$. Chorus and magnetosonic waves were detected and removed from the data set by hand inspection (Tsurutani et al., 2014). The Polar Plasma Wave Instrument (Gurnett et al., 1995) data were used to determine the plasmaspheric hiss intensities and occurrence rates as a function of L and MLT. The average wave log intensities as a function of L and MLT were used for the statistical studies.

For the statistical surveys, the ~2-kHz bandwidth High Frequency Waveform Receiver data were used. This data cover the frequency range ~300 Hz to ~1.0 kHz in six frequency band steps, obtaining a ~0.4-s snapshots for every ~2-min interval (Santolik et al., 2001). The ~2-min intervals were then used as the main elements for our statistical studies. These will be called *intervals* in the text. If plasmaspheric hiss is detected during an interval, it is called a *wave event*. Data were binned by L and MLT with a bin size of 1-L by 1-hr MLT. The average plasmaspheric hiss crossing event was ~92 min, with a minimum of ~6 min and a maximum of ~224 min. It should be noted by the reader that these time interval values are due to a combination of the satellite trajectory through the wave region and the hiss duration. The detected emissions themselves can last tens of minutes to hours. No one presently knows the exact values because of single spacecraft orbital limitations. Thus, our ~2-min samples are not statistically independent. The reader should be aware of this in interpreting our results/conclusions.

In this ~1-year statistical study, Polar crossed the plasmasphere over 1,000 times. Of the total, ~800 passes occurred when the Polar ~2-kHz wave data were available. Each pass consists of many ~2-min intervals and thereby many potential wave events. These latter ~800 passes with many ~2-min intervals are the basis for the statistical part of this study.

This study will focus on the 10 most intense ~2-min wave events in each of four local time sectors. We will analyze both the specific ~2-min wave event and also the plasmaspheric hiss throughout the Polar satellite pass for that particular event. Thus, once an intense ~2-min event was identified, the ~2-min interval before and after and so on were studied to have the whole plasmaspheric hiss data for that satellite pass. This satellite pass data will be called an *intense plasmaspheric hiss interval*. The purpose is to characterize the plasmaspheric hiss at different local times. This information will be used to help identify possible sources of the waves. It should be mentioned that since the 10 events are taken during different Polar passes, these events are statistically independent.

For case studies, we use the high time resolution ~0.4-s plasma wave data. The minimum variance method (Smith & Tsurutani, 1976) is used to determine the wave k and the direction of wave propagation (Verkhoglyadova et al., 2010). From the k direction and the magnetic field direction Bo (determined from the d.c. magnetometer), the wave polarization will be obtained.

The wave coherence is analyzed for the above 40 cases of 10 maximum wave intensities (in the four MLT sectors). A cross correlation of the B1 (maximum variance) and B2 (intermediate variance) components of the magnetic wave was performed on the entire ~0.4-s interval, on a selected five-wave cycle sample of each event, and on the individual five-wave cycles. This was done for all forty ~0.4-s intervals. We will present only a short summary of the findings for purposes of brevity.

The year of study occurred during the solar minimum phase of the solar cycle. During this phase, there is typically a paucity of intense Interplanetary Coronal Mass Ejection (ICME)-generated magnetic storms (Gonzalez et al., 1994; Tsurutani et al., 2006; Tsurutani, Echer, et al., 2011). High-speed stream-slow speed stream interactions form Corotating Interaction Regions at their interface (Smith & Wolfe, 1976). The Corotating Interaction Regions can cause weak magnetic storms (Tsurutani et al., 1995). However, the high-speed streams themselves are the dominant interplanetary feature resulting in geomagnetic activity during this
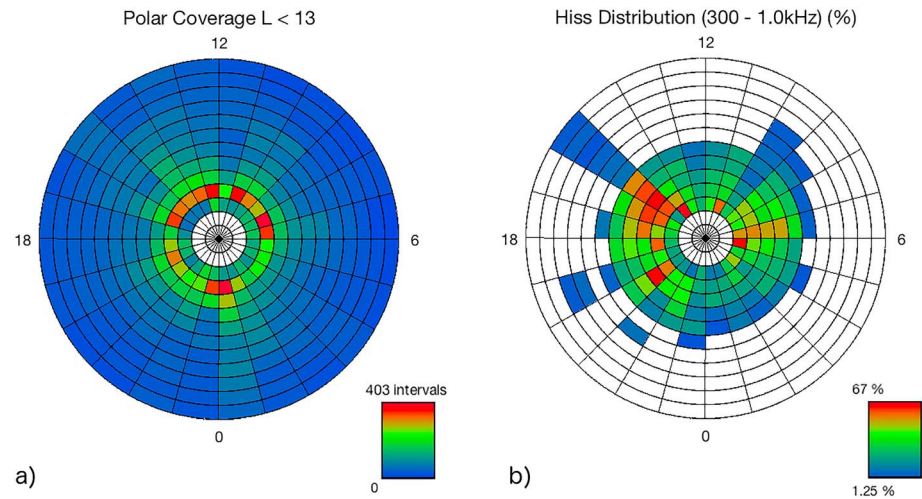
Figure 1. (a) Polar satellite coverage for the study, given as a function of L and MLT. Noon is on the top, and dawn is on the right. The coverage extends from L = 2 to L = 13. The legend gives the number of ~2-min intervals for each ΔL-ΔMLT bin. (b) The plasmaspheric hiss occurrence frequencies for ~300-Hz to ~1.0-kHz waves. Each bin size is 1-hr MLT and 1 L-shell. The color code on the lower right gives the occurrence percent frequencies. MLT = magnetic local time.

part of the solar cycle. The embedded Alfvén wave southward Interplanetary Magnetic Field (IMF) components within the high-speed streams can cause High-Intensity Long-Duration Continuous AE Activity (HILDCAA) events (Hajra et al., 2013, 2014; Tsurutani et al., 2006; Tsurutani & Gonzalez, 1987). HILDCAAs are a series of intense substorms/small injection events with concurrent midnight sector plasmasheet injections that occur continuously for days to weeks.

We will statistically study the 40 plasmaspheric hiss events using the solar wind ram pressure from solar wind velocity and density measurements taken from the OMNI website. Since solar wind pressure has an immediate effect on the dayside outer magnetosphere and the energetic ~10–100-keV electrons therein, no further time delays were used. When we consider plasmaspheric hiss associated with substorms and plasma injection events, we need to determine the AE and SYM-H values assuming midnight injection and gradient drift of the energetic electrons to the local time of detection. For this part of our study, we will assume a model of gradient drift of ~25-keV electrons. This model was found to be a good measure of chorus delay times by Tsurutani and Smith (1977) and more recently by Falkowski et al. (2017). It should be noted that HILDCAA intervals have been shown to be a mixture of continuous substorms and injection events (Tsurutani et al., 1995, 2004). HILDCAAs are therefore not simply isolated *substorms*. Although not part of the scope of this paper, it should be mentioned that the details of these *injection events* have yet to be identified.

The solar wind data were obtained from the OMNI website (http://omniweb.gsfc.nasa.gov/). These data are time adjusted to take into account the solar wind propagation time from the spacecraft to the magneto-sphere, so no further adjustments were made to the data. The AE and SYM-H data were obtained from the WDC at Kyoto University (http://wdc.kugi.kyoto-u.ac.jp/wdc/Sec3.html). In studies done in this paper, we will use precursor AE and SYM-H values which we will refer to as AE* and SYM-H*.

3. Results

3.1. Data Coverage and Plasmaspheric Hiss Data Set

Figure 1 shows the Polar satellite coverage (Figure 1a) and the plasmaspheric hiss average occurrence frequency for the year of data analysis study (Figure 1b). Polar has an elliptical orbit with perigee at ~2 Re from the center of the Earth and apogee at ~9 Re. The orbital period is ~17.5 hr. Figure 1b is for the plasmaspheric hiss frequency range of ~300 Hz to ~1.0 kHz, the focus of the present study. Here we have limited the L range from 2 to 13.

The principal feature to be noted from Figure 1a is that all L and MLTs are well covered by the Polar satellite transits and ~2-min intervals of data. Figure 1b shows that the greatest plasmaspheric hiss occurrence frequency occurs in the dusk sector. In the region between L = 2 and 7 at all MLTs, plasmaspheric hiss was
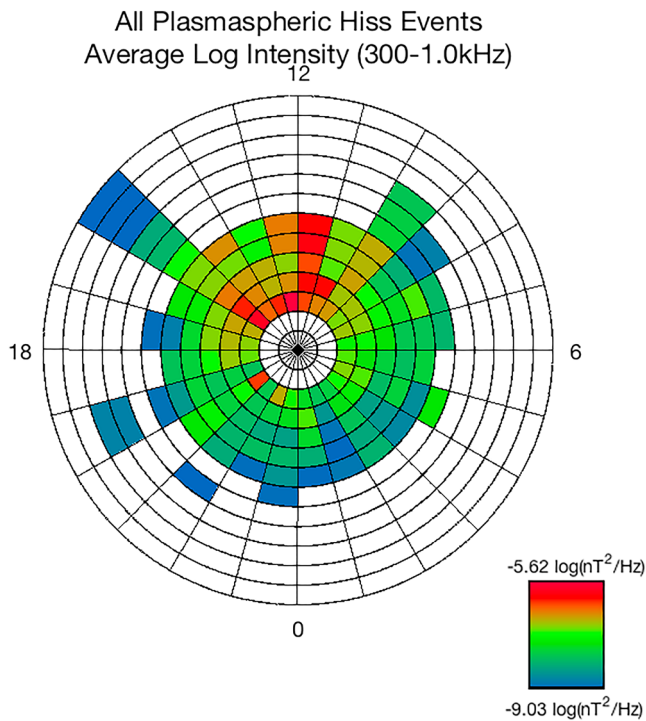
Figure 2. Approximately 300-Hz to 1.0-kHz plasmaspheric hiss average log intensity as a function of L and MLT. The same format as in Figure 1.

detected 32% of the time. In the dusk sector from L = 3 to 6 and 15 to 21 MLT, plasmaspheric hiss was detected 51% of the time.

Figure 2 shows the average plasmaspheric log intensity as a function of L and MLT. Plasmaspheric hiss is found to be most intense on the dayside sector of the plasmasphere. The bin size for averaging was ΔL = 1 and ΔMLT = 1. The intense waves (red) extend out to L = 7. This is a duplication of the Falkowski et al. (2017) result. However, it is noted that Falkowski et al. also examined LF hiss in the range ~22 to 100 Hz and found no local time asymmetry. For this reason (and others stated previously), we have excluded LF plasmaspheric hiss in this present study.

It should be noted that in Figure 2, there are many plasmaspheric hiss intervals that occur outside of L = 6 to 7, the normal location of the plasmapause. These waves are thought to be associated with hiss inside of plasmaspheric plumes or tails (Summers et al., 2008; Tsurutani et al., 2015). From detailed analyses, these waves were found to be both coherent and of high intensity. It is noted from this figure that their intensities are lower than the maximal intensities that occur in the noon sector. We will comment on this further later in the paper.

Figure 3 shows the ~300 Hz to ~1.0 kHz 40 most intense ~2-min plasmaspheric hiss average log intensity interval locations in L and magnetic latitude (MLAT). As mentioned previously, the 40 events are composed of the top 10 events for each of four local time sectors: midnight, dawn, noon, and dusk. What is interesting in this figure is that there is a cluster of intense (red) points at low L (~2.9 to 3.4) within ~18° of the magnetic equator. Another feature that should also be noted is that intense plasmaspheric hiss is also detected beyond 50° MLAT.

Figure 3b shows the spacecraft L-MLAT coverage. It is noted that Polar covers the magnetic equator well between L = ~2.4 and ~4.3 but not for higher L. At L = 6 to 7 (the nominal plasmapause location), Polar covers the MLAT range of ~20° to ~40° well. However, at lower and higher MLATs outside this range, the coverage is poor to nonexistent.

The plasmaspheric hiss data in Figure 3a have not been normalized. However, one can note from the spacecraft tracks given in Figure 3b that the greater number intense emission events detected at low L near the magnetic equator might be an artifact of a greater number of spacecraft passes through that region of phase space.
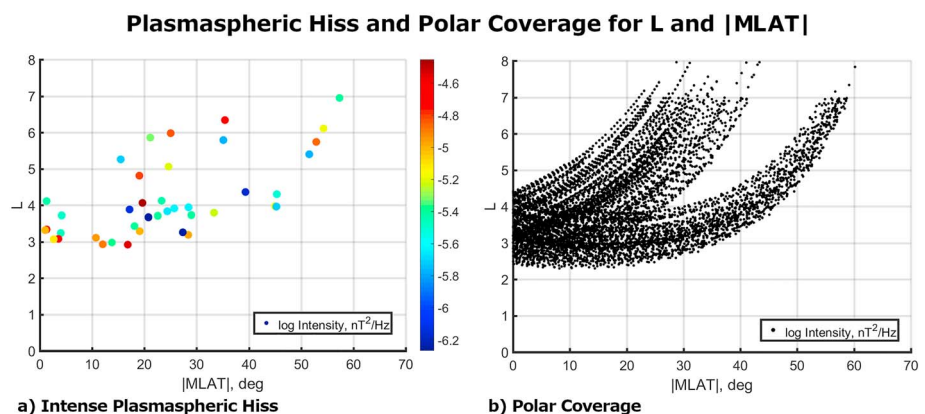
Figure 3. (a) shows the distribution of the 40 most intense ~2-min intervals of plasmaspheric hiss. (b) gives the spacecraft coverage for this data survey. MLAT = magnetic latitude.
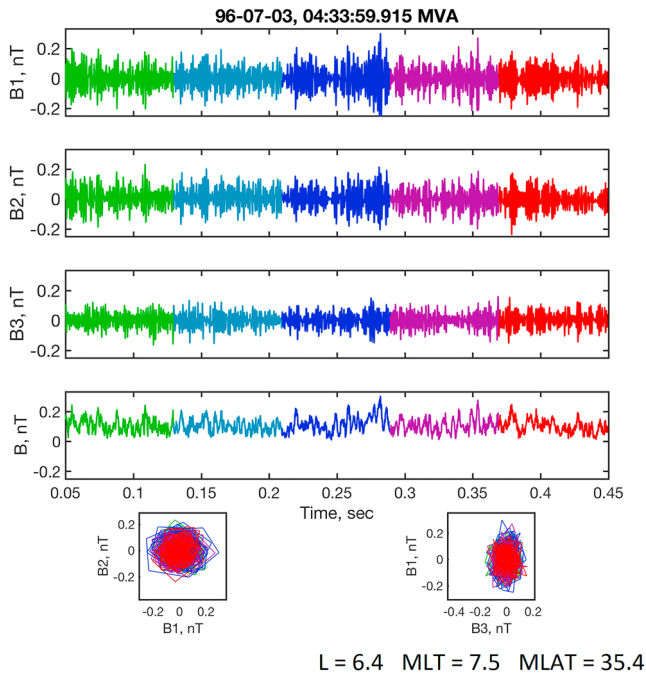
Figure 4. A ~0.4-s interval with circularly polarized plasmaspheric hiss. Five different colors have been added at equal time intervals to allow the reader to follow the evolution of the waves. MVA = minimum variance analysis; MLT = magnetic local time; MLAT = magnetic latitude.

3.2. The Properties of the 10 Most Intense Plasmaspheric Hiss ~2 min in the Four MLT Sectors

The 10 most intense ~2-min average hiss intervals for each of the four MLT sectors were identified. Thus, 40 intervals were examined in detail. Each interval was found to be composed of small intervals (approximately three to five cycles) of coherent to quasi-coherent waves. There were no intervals of totally incoherent waves detected within the forty ~2-min intervals studied. Thus, it is possible that even lower intensity plasmaspheric hiss is also coherent to quasi-coherent in nature. However, this is beyond the scope of the present work and will not be discussed further.

All of the clearly identifiable waves were right-hand polarized. The whole range of polarizations, circular, elliptical, and linear was detected. There is no apparent local time dependence on these three general polarizations. Examples of each of these three types of right-hand wave polarizations are shown below.

### 3.3. Polarizations of Whistler Mode Plasmaspheric Hiss

Figure 4 is an example of circularly polarized plasmaspheric hiss. The ~0.4-s interval occurred at L = 6.4, an MLT of 7.5 hr (local dawn sector), and a MLAT of 35.4°. The event started on 3 July 1996 at ~0433:59.915 UT. From top to bottom are the wave magnetic field B1 (max variance) component, the B2 (intermediate variance) component, the B3 (minimum variance) component, and B magnitude. The bottom left box displays the B1-B2 hodogram and the bottom right box the B1-B3 hodogram.

The top two panels which contain the B1 and B2 magnetic field components show that the two components have essentially the same amplitudes. The B3 variations (third panel from the top) have substantially lower amplitudes than either B1 or B2. These features are consistent with circular polarized waves. The bottom left hodogram confirms this average picture. The hodogram on the bottom right shows that the waves are either a mix of planar waves propagating nearly parallel in direction or slightly nonplanar waves.

To examine this further, a five-wave cycle interval from Figure 4 is shown in Figure 5. The start of the interval is at 0433:60.140 UT. The left-hand panels (Figure 5a) are given in the same format as in Figure 4. The B1 and B2 wave amplitudes are approximately the same, with a wave phase shift between the two
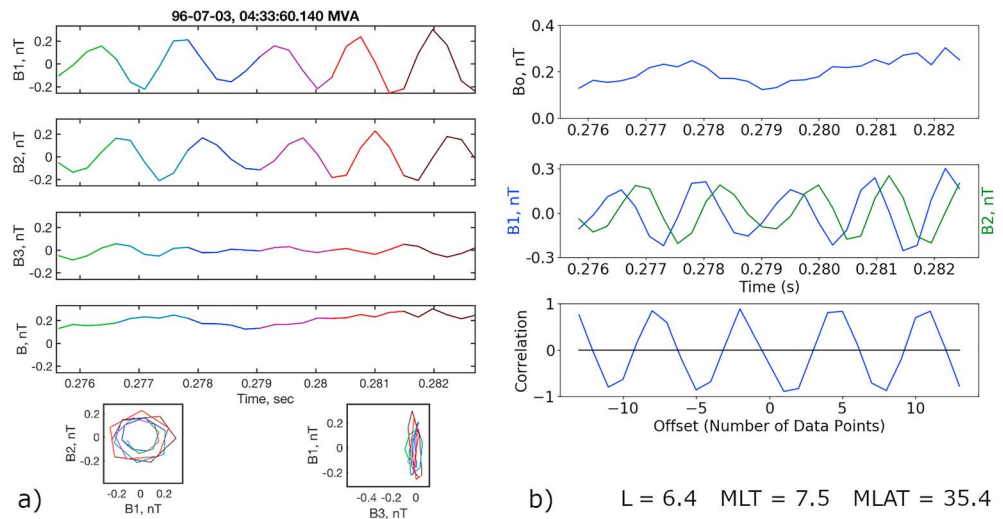
Figure 5. (a) Five cycles of plasmaspheric hiss in the same format as in Figure 4. Five different colors for equal time intervals have been used to allow the reader to follow the wave progression. At the bottom of (a) are the B1-B2 hodogram and the B2-B3 hodogram. (b) gives the field magnitude, the B1 and B2 components superposed, and the cross correlation of B1 and B2 results. MVA = minimum variance analysis; MLT = magnetic local time; MLAT = magnetic latitude.
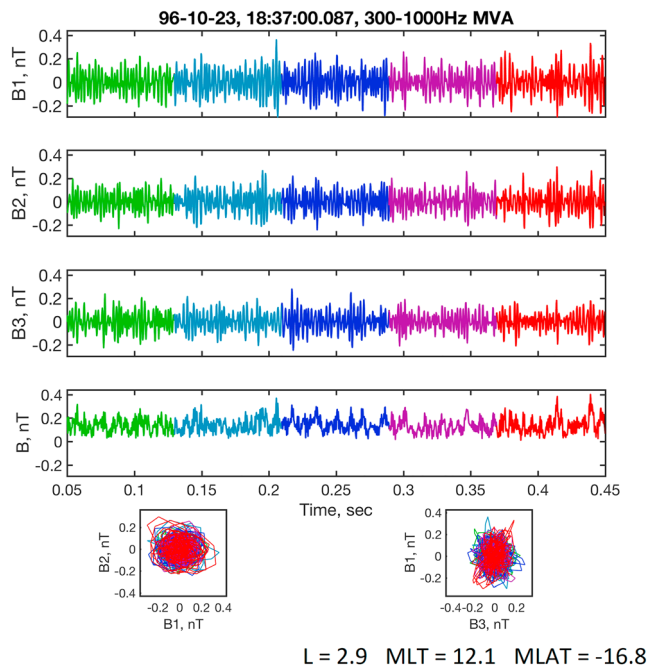
Figure 6. A ~0.4-s interval that contains elliptically polarized plasmaspheric hiss. The format is the same as in Figure 4. MVA = minimum variance analysis; MLT = magnetic local time; MLAT = magnetic latitude.

components of approximately 90°, as expected for circularly polarized electromagnetic waves. The B1-B2 hodogram at the bottom left confirms that the wave polarizations are circular. The B1-B3 hodogram indicates that these are planar waves.

Figure 5b from top to bottom gives the magnetic field magnitude, B1 and B2 components (plotted superposed in the same panel), and the cross correlation between B1 and B2. The bottom graph clearly shows that the waves are coherent with a ~0.9 cross-correlation coefficient.

Figure 6 is a 0.4-s interval that started at 1837:00.087 UT on 23 October 1996. The spacecraft location was at L = 2.9, MLT =12.1 (noon sector), and a MLAT of −16.8°. The format is the same as in Figure 4.

In Figure 6, the B1 fluctuations are slightly larger than the B2 fluctuations. The B2 and B3 fluctuations are nearly equal. The B1-B2 hodogram shows that there are mainly circularly polarized waves present with some elliptical polarization. The B1-B3 hodogram indicates that the polarizations are varying with time. However, neither of these latter two points is totally clear from these hodograms. Thus, a five-wave cycle interval is analyzed again (Figure 7).

Figure 7 gives an example of five cycles of elliptically polarized waves starting at 1837:00.474 UT in Figure 6. It can be noted from the B1 and B2 magnetic components in Figure 7a that B1 has a larger amplitude than B2. The B1-B2 hodogram at the bottom clearly indicates that the waves are elliptically polarized with a ratio of ~2 to 1. The B1-B3 hodogram shows that the waves are planar.

The right-hand bottom panel of Figure 7b shows a cross-correlation coefficient of ~0.95 when the lag is approximately one-fourth wavelength. These waves are highly coherent. For longer lags, the correlation coefficient decreases to 0.7 to 0.8. This feature will be discussed in more detail later in the paper.

Figure 8 shows a ~0.4-s interval of linearly polarized plasmaspheric hiss starting at 1112:02.343 UT on 18 November 1996. The location was L = 3.2, an MLT of 10.1 (noon sector), and a MLAT of −28.4°. From this figure, it can be noted that the B1 component variations are much larger than either the B2 or B3 variations. The latter two variations are comparable in amplitude. The B1-B2 hodogram indicates that the waves are elliptically polarized or linearly polarized with some variation in polarization planes. The B1-B3 hodogram is difficult to interpret for this linear wave case.
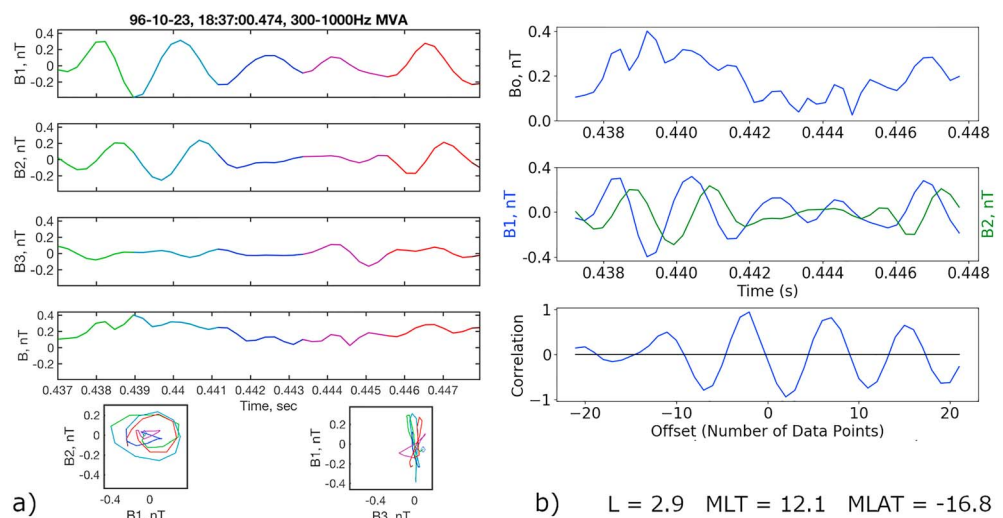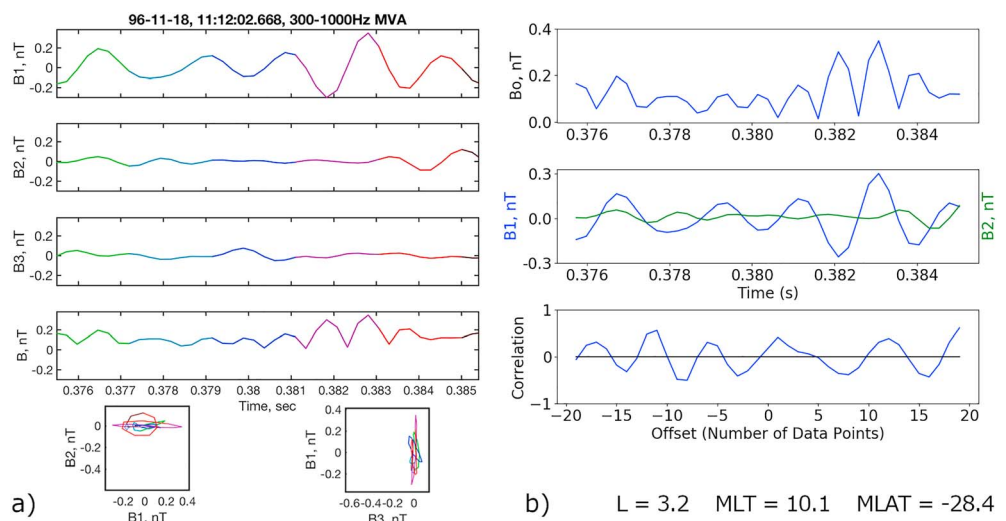

Figure 7. Same format as in Figure 5. An example of five cycles of elliptically polarized waves. MVA = minimum variance analysis; MLT = magnetic local time; MLAT = magnetic latitude.
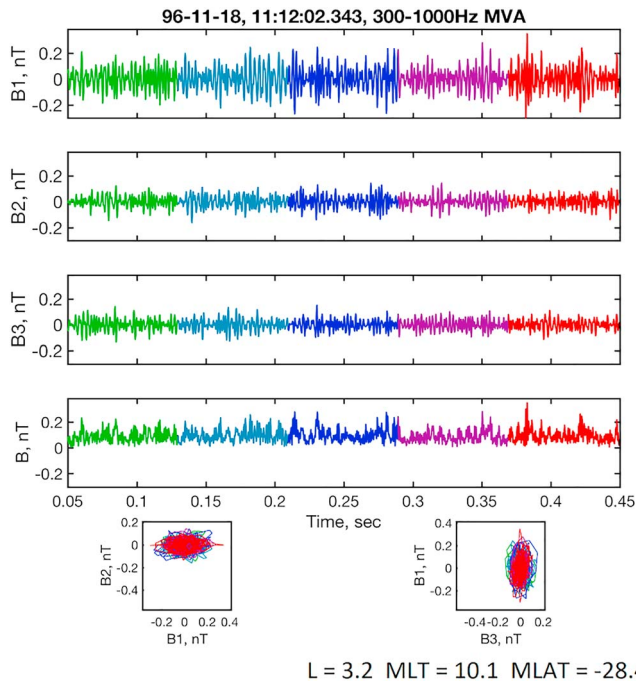
Figure 8. A ~0.4-s interval of linearly polarized plasmaspheric hiss. The format is the same as in Figure 4. MVA = minimum variance analysis; MLT = magnetic local time; MLAT = magnetic latitude.

Figure 9 shows a five-cycle interval of linearly polarized plasmaspheric hiss from the same time interval, 18 November 1996 starting at 1112:02.668 UT. The B1 component of Figure 9a is substantially larger than that of the B2 component. The B1-B2 hodogram at the bottom clearly shows the nature of the linearly polarized waves. There is a circularly polarized wave cycle at the very end of the interval.

The bottom data trace in Figure 9a gives the magnetic field magnitude. There are substantial variations in the wave field magnitude with periods half that of the B1 wave. This indicates that the magnetic oscillations are along the ambient magnetic field causing the substantial compressive variations.

One might ask the question could this be a magnetosonic wave interval instead of plasmaspheric hiss? At a distance of L = 3.2 and a MLAT = −28.4°, the standard generation mechanisms for magnetosonic wave generation would be difficult to invoke (see Horne et al., 2000; Perraut et al., 1982; Santolik et al., 2002; Tsurutani et al., 2014). For magnetosonic waves, the wave magnetic oscillations are also along Bo. Most typically, there are little or no oscillations in the other components. Here there are very few variations in B2 except at the tail end of the interval (second panel in Figure 9a). This is the circularly polarize wave cycle. This circular wave can be noted in the bottom left B1-B2 hodogram.

Figure 9b, bottom panel, shows the B1-B2 cross correlation. The maximum value is ~0.6. This wave interval is quasi-coherent.

3.4. Statistics of the 40 Intense *Event Intervals*

The 10 most intense plasmaspheric hiss events during each of four local time sectors were identified and discussed above. It was also previously noted that plasmaspheric hiss detected by Polar could last from 6 min to 3.7 hr with a mean duration of 1.5 hr. Thus, each of the forty ~2-min intervals of intense plasmaspheric hiss was not isolated. Plasmaspheric hiss was detected in the ~2 min prior and in the ~2 min after the intense ~2-min interval wave events. For each of the 40 intense ~2-min events, we traced the plasmaspheric hiss for that particular satellite inbound or outbound pass. We call this total accumulation of consecutive ~2-min events, the plasmaspheric hiss event interval. We will now discuss the properties of the plasmaspheric hiss in the 40 event intervals.

Figure 9. A linearly polarized plasmaspheric hiss event. Same format as in Figure 5. MVA = minimum variance analysis; MLT = magnetic local time; MLAT = magnetic latitude.

The Top Ten Most Intense Hiss Events in Each of Four Time Sectors (300-1.0kHz)
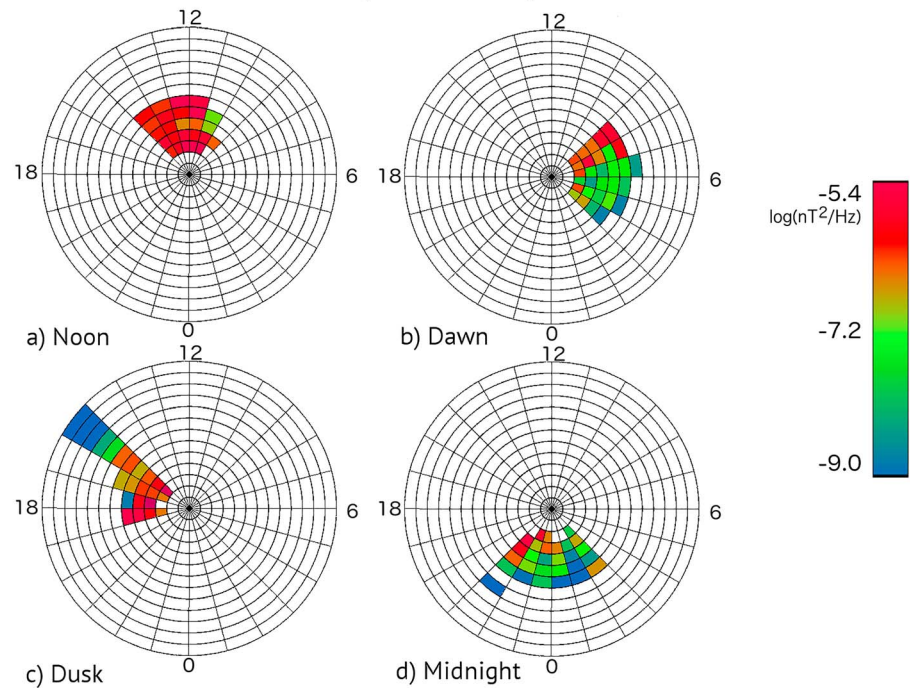

Figure 10. The top 10 plasmaspheric hiss *event intervals* for (a) the noon sector, (b) the dawn sector, (c) the dusk sector, and (d) the midnight sector. The format is the same as in Figure 2.

Figure 3 showed the top 10 most intense plasmaspheric hiss ~2-min events in log intensity for each of four local time sectors. Figure 10 shows the distribution of the event intervals. By the event intervals, we mean all of the plasmaspheric hiss ~2-min events along that spacecraft track.
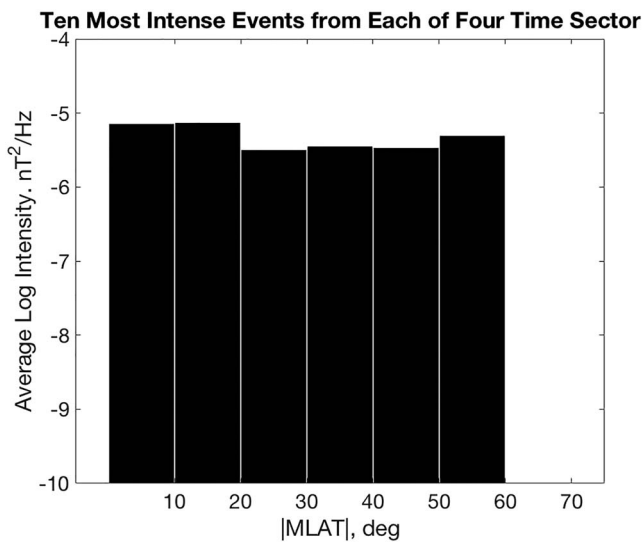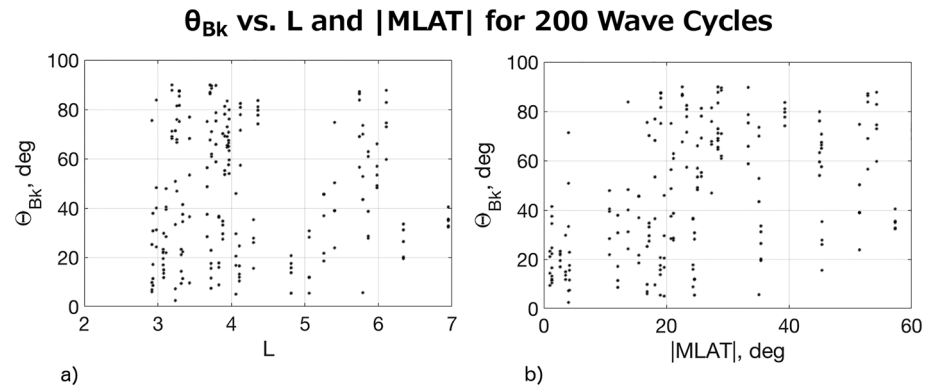
The most (average log) intense (red) plasmaspheric hiss regions are found throughout the noon sector. The intense waves are found for L < 7. Intense plasmaspheric hiss is also detected for the first 2 hr (7 to 9 MLT) of the dawn sector also inside L = 7. There is a region of intense waves detected in the dusk sector from 15 to 19 MLT inside L = 5. The dusk sector shows an extended feature in L from 15 to 16 MLT. As mentioned previously, this is most likely hiss associated with a plasmaspheric tail (A. J. Chen & Grebowsky, 1974). It should be noted that the waves are most intense inside L = 8 and less intense in the region 8 < L < 13. This is the same dependence previously noted in Figure 2 for the general case of plasmaspheric hiss.

The MLT sector with the weakest intensity plasmaspheric hiss is local midnight. Similar features were found in Tsurutani et al. (2015). This was explained by the idea that magnetospheric chorus in the midnight sector is present only near the magnetic equator (Meredith et al., 2001; Tsurutani & Smith, 1974, 1977). The waves are presumably strongly Landau damped as they propagate away from the equatorial generation region to higher latitudes (however, opposite arguments are presented later in why there is hiss in the midnight sector during solar wind pressure events later). Assuming that chorus is the source for plasmaspheric hiss, the chorus will typically not reach high magnetic latitudes to be able to enter the plasmasphere.

Figure 11. The average plasmaspheric hiss log intensity as a function of absolute magnetic latitude. This survey was taken over all magnetic local times. MLAT = magnetic latitude.

θ_{Bk} vs. L and |MLAT| for 200 Wave Cycles

a)   b)

Figure 12. (a) Wave normal angle θ_{kB} as function of L and (b) θ_{kB} as a function of MLAT. The 200 individual wave cycles analyzed are shown in this figure. MLAT = magnetic latitude.

Each of the four MLT sectors were first studied independently. All four sectors showed essentially the same features that there was no obvious intensity dependence on magnetic latitude. Thus, all four MLT sectors have been put together for Figure 11. There is very little or no dependence on log intensity as a function of magnetic latitude. This result is somewhat surprising and in contrast to the finding of Meredith et al. (2018). This will be discussed later.

### 3.5. A Summary of Plasmaspheric Hiss Properties for the 40 Wave Events

As previously mentioned, for each of the 40 maximum wave intensity events, five consecutive individual wave cycles were analyzed. Examples of circularly polarized waves (Figures 4 and 5), elliptically polarized waves (Figures 6 and 7), and linearly polarized waves (Figures 8 and 9) were shown previously. For all 40 five-wave cycle intervals (200 cycles total), each wave cycle was further analyzed. Some of the results of this detailed analysis is shown in Figure 12, the wave angle of propagation relative to the ambient magnetic field direction, θ_{kB}.

Figure 12a shows θ_{kB} as a function of L. Figure 12b gives θ_{kB} as a function of absolute MLAT. The main finding is that there is no strong dependence of θ_{kB} on either plasmasphere location parameters. There might be a slight dependence of θ_{kB} on |MLAT| shown in Figure 12b. For |MLAT| $< 20°$, most waves have $\theta_{kB} < 40°$. Higher θ_{kB} values are detected at higher |MLAT| values. If there was a simple single source of chorus which is propagating first to high magnetic latitudes (low altitudes) and into and throughout the plasmasphere as indicated by Bortnik, Li, et al. (2009) and Bortnik et al. (2011), then one would expect to see some definite order of the plasmaspheric hiss wave angle of propagation in L and MLAT. The results of Figure 12 might be explained by the existence of many chorus sources (at a variety of L), propagating into the plasmasphere. The waves may be refracting and also making multiple passes. There are other interpretations as well. The one positive finding of this result is that this might simplify wave-particle interaction modeling. This finding will be discussed further later in the paper.

The wave cycles were separated into circularly polarized, elliptically polarized, and linear polarized cycles. The three types of polarizations were divided into 10° θ_{kB} bins. The results are shown in Figure 13.

Figure 13 shows that most of the intense event wave cycles were elliptically polarized (Verkhoglyadova et al., 2010). This feature is present at all angles of wave k relative to the ambient magnetic field. Circularly polarized waves were also present at all θ_{kB} angles and were most prominent at low angles, $10° \leq \theta_{kB} \leq 40°$. Linearly polarized waves were present only for $\theta_{kB} \geq 50°$.
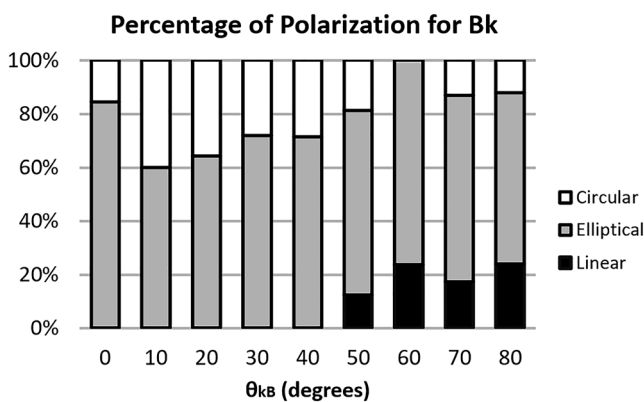
Figure 13. The percent circular, elliptically, and linearly polarized plasmaspheric hiss as a function of angle of wave k relative to the ambient magnetic field direction (B).
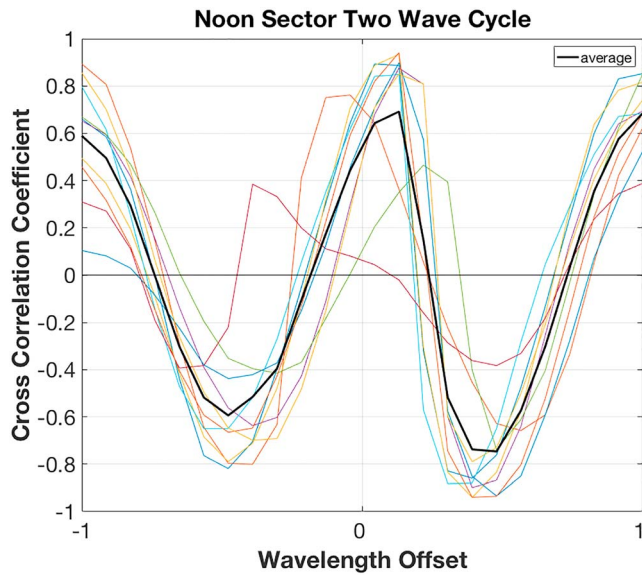
Figure 14. Two-wave cycles from each of the 10 most intense noon sector five-wave cycle intervals. The plot is the cross-correlation results from the wave B1 and B2 minimum variance components.

A quantitative estimate of the wave coherency for the 10 most intense event wave cycles for each of the four local time sectors was sought. What was done is to take two wave cycles from each of the 10 five-wave cycle intervals, adjust their wavelength to match a common size, and then superpose them together. Figure 14 shows the results for the noon sector events.

Figure 14 shows the wave coherence for each of the 10 intense events detected during the noon sector. The individual events are shown by color, and the average value is shown as the black curve. It can be seen that the average correlation at one-fourth wavelength shift (near 0 on the horizontal axis) is ~0.8, and it remains at approximately that value for a further shift of one wavelength (+1 wavelength offset) and a negative one wavelength offset (−1 wavelength offset). Thus, these waves are coherent over two cycles at least.

3.6. Substorms and Small Injection Events

The plasmaspheric hiss AE* distributions of the 40 intense event intervals are shown in Figure 15 in white and gray tones. The time adjustments were made between AE and AE* assuming a gradient drift time of ~25-keV electrons assuming a local midnight injection of the particles. The scale is given on the left as percent occurrence. The black background distribution is AE for the year of study. This scale is the same for the percentage of 1-min data points. It is clear that the two distributions are fairly similar. The main difference is that there is some hint that plasmaspheric hiss occurs at middle AE* values (270 to 360 nT) and very high AE* values (~540 to 780 nT) than the yearly distribution. Thus, intense plasmaspheric hiss seems to have a slight substorm dependence.
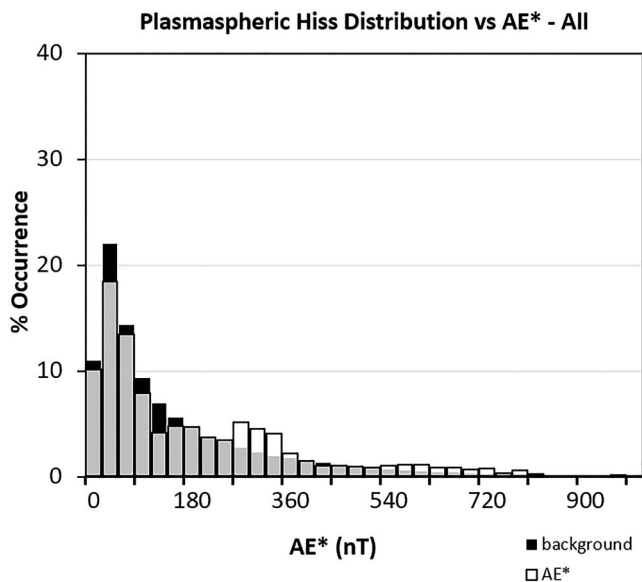
Figure 16 shows the intense plasmaspheric hiss AE* distributions in four local time sectors. The top three panels are (a) midnight sector, (b) dawn sector, and (c) noon sector. The bottom panel, (d), shows the AE* distribution for the plasmaspheric hiss in the dusk sector. The format is the same as in Figure 15, with the plasmaspheric hiss given in percent occurrence in white/gray. The percent AE for the year of study is given in black.
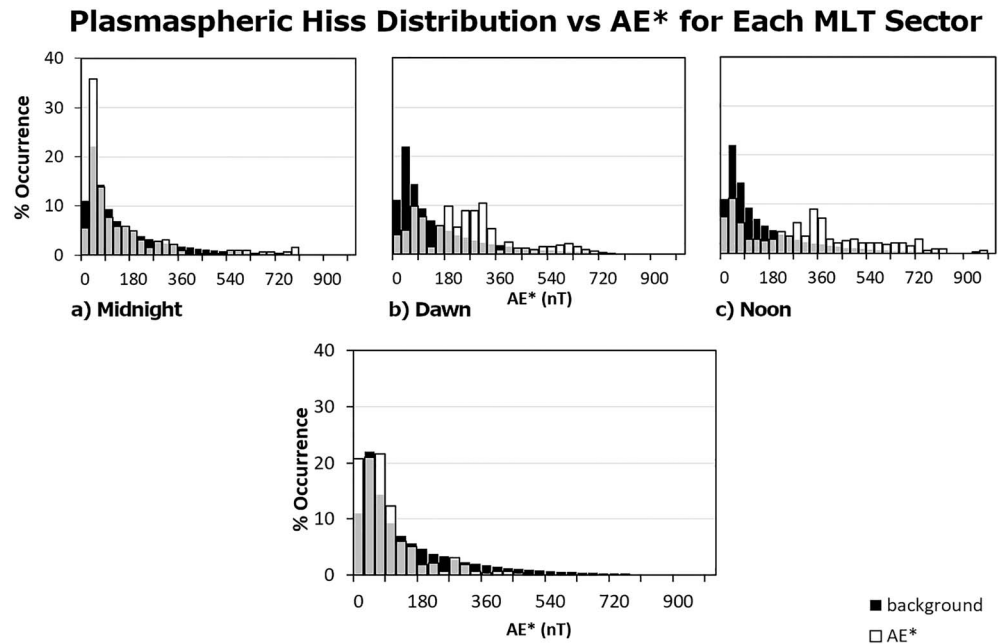
The distribution of percent AE* occurrence is different at the four local time sectors. On the top showing the dawn and noon sectors, the plasmaspheric hiss percent occurrences indicate strong AE* dependences. The distributions are weighted toward much higher AE* than the background AE normalized distribution. The midnight sector in Figure 16a is a bit different. There is a preponderance of events occurring at low AE* values, AE less than ~90 nT. However, there is a small amount of high intensity AE* events. This will be addressed again later.

In Figure 16d, the dusk sector shows little to no plasmaspheric hiss AE* dependence. The percent occurrence distribution is oriented to low AE* values, even lower than that of the AE (background) distribution.

Figure 15. The normalized percent distribution of all local time sectors of plasmaspheric hiss event interval AE* values (white/gray tone bars) and the percent occurrence of AE for the year of study (black). The scale for both the plasmaspheric hiss and the AE background is given on the left.

One simple interpretation of the results of Figure 16 is that these distributions correspond to the distributions of outer zone magnetospheric chorus. Chorus has been typically detected in the midnight, dawn, and noon sectors with a general absence in the dusk sector (Meredith et al., 2001, 2012; Tsurutani & Smith, 1977). It is also noted that the drift of ~10- to 100-keV midnight sector substorm injected electrons go from midnight through dawn to noon. One possibility is that the electron-free energy is depleted by the time that they pass the noon sector, and generation of chorus is terminated. This will be discussed in more detail later.
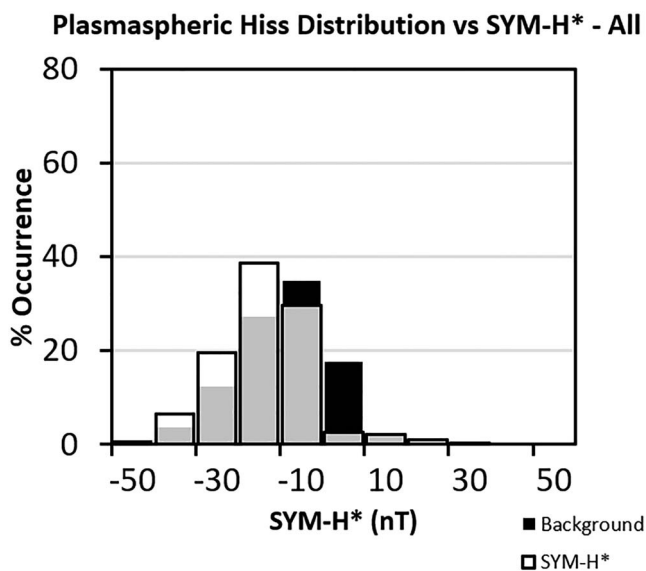
Figure 16. The same format as in Figure 15 but for all four local time sectors separately. (a) shows the AE* distribution of plasmaspheric hiss in the midnight sector, (b) plasmaspheric hiss in the dawn sector, and (c) plasmaspheric hiss in the noon sector. (d) displays plasmaspheric hiss in the dusk sector. The AE distribution for the year of study is shown in black in each panel. MLT = magnetic local time.

The general lack of midnight sector chorus away from the magnetic equator (outside of ±15° MLAT; Tsurutani & Smith, 1974) has been interpreted as strong off-axis Landau damping. This may explain the lack of plasmaspheric hiss in this local time sector.


Figure 17. Same general format as in Figure 15 but for plasmaspheric hiss event interval SYM-H* values for all local time sectors. The SYM-H* plasmaspheric hiss histogram is given in white/gray with the annual background SYM-H in black. The percent occurrence scale is on the left.

Figure 17 shows the distribution of SYM-H* values of all plasmaspheric hiss 40 intense event intervals in white/gray. The normalized percent occurrence scale is shown on the left. Again, similar to the AE* calculations, the SYM-H* value calculations assume a midnight injection of ~25-keV electrons and gradient drift to the MLT of observation. The SYM-H 1-min value percent occurrences for the year of study are shown in black.

The intense plasmaspheric hiss SYM-H* distribution has a slightly stronger negative SYM-H* component and a lesser positive SYM-H* component. This result implies that these very intense plasmaspheric hiss events are oriented more toward geomagnetic activity than toward solar wind pressure pulse events. However, the above results might be local time sector dependent. We will show that next.

Figure 18 gives the plasmaspheric hiss event interval SYM-H* percent occurrence distributions for the four MLT sectors separately. The format of each panel is the same as that in Figure 16 but for SYM-H* values. Two of the top three panels, that of (a) dawn and (b) noon, indicate that the intense 10 event intervals were associated with negative SYM-H* intervals. Surprisingly, it is noted that at noon, very few of the 10 events were associated with positive pressure SYM-H* values. This is quite different than for plasmaspheric hiss in general (Falkowski et al., 2017). Since these SYM-H* values are not less than −50 nT, the geomagnetic activities are not magnetic storms (Gonzalez et al., 1994) but most likely associated with shallow substorm injection events, such as HILDCAA intervals (Tsurutani

Plasmaspheric Hiss Distribution vs SYM-H* for Each MLT Sector
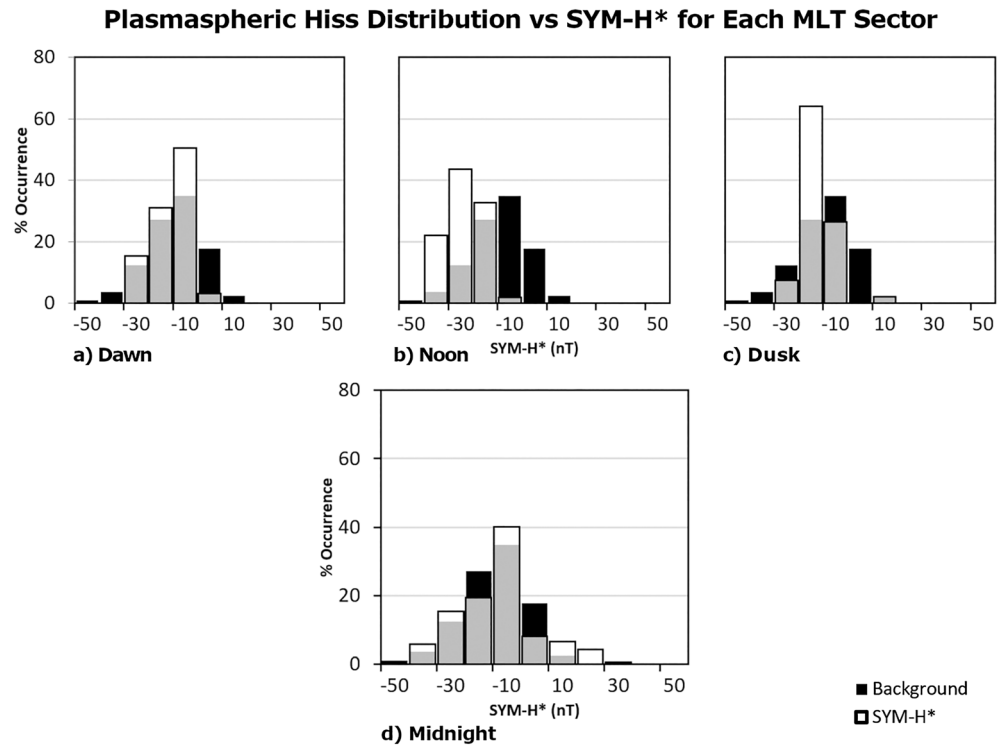
Figure 18. Plasmaspheric hiss SYM-H* value distributions for the four MLT sectors. On the top are the (a) dawn sector, (b) noon sector, and (c) dusk sector, and on the bottom is the (d) midnight sector. Plasmaspheric hiss normalized percent occurrence is given in white/gray, and the year background SYM-H is given in black. MLT = magnetic local time.

et al., 2006). The dusk sector in Figure 16c shows both negative SYM-H* dependence and some positive SYM-H* dependence.
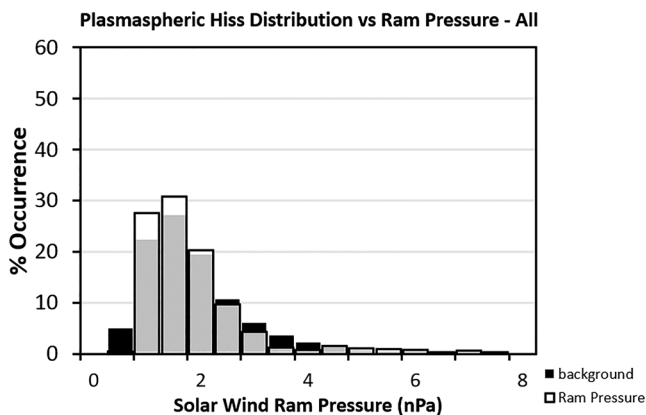
These results in Figure 18 are, in general, consistent with the plasmaspheric hiss substorm dependence results of Figure 16. It should be noted that for the noon sector results, there are only a few positive SYM-H* values, perhaps indicating a lack of solar wind ram pressure dependence. However, SYM-H* is a time-advanced index, and in this figure, the SYM-H is not taken at the same time as the plasmaspheric hiss is taken. A more accurate method would be to compare the measured solar wind ram pressure which will be examined next in this paper.
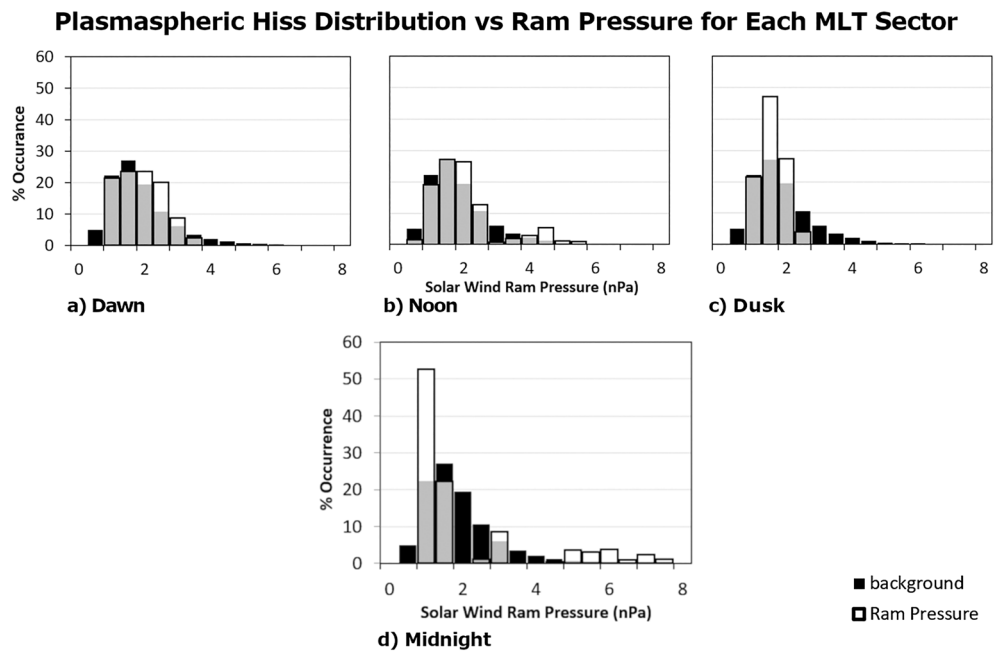
What is unexpected in distribution is that of the plasmaspheric hiss percent occurrence distribution in the midnight sector, Figure 18d. In this panel it is apparent that some of the waves were associated with high positive SYM-H* values. Some of the plasmaspheric hiss also occurred at negative SYM-H* values.

Figure 19. Same general format as in Figure 15 but for plasmaspheric hiss event interval solar wind ram pressure for all local time sectors. The solar wind ram pressure-hiss histogram is given in white/gray with the scale on the left. The plasmaspheric hiss distribution is normalized to 100%. The solar wind ram pressure 2-min average percent occurrences for the year of study is shown in black.

Figure 19 gives the solar wind ram pressure during the intense plasmaspheric hiss event intervals. This has been done for all local times. The plasmaspheric hiss is shown in white/gray bars, and the annual solar wind ram pressure distribution is shown in black. It can be noted that some of the intense plasmaspheric hiss studied in this paper have occurred during high solar wind pressure intervals, with Psw > 4.5 nPa.

Falkowski et al. (2017) showed that the dayside sector plasmaspheric hiss was related to both solar wind ram pressure and to substorms (with delay of gradient drifting ~25-keV electrons). So part of the result in Figure 19 is expected for the highest intensity waves as well. However, here the

Figure 20. Same format as Figure 19 but the four local time sectors are analyzed separately. (a)–(d) correspond to the dawn, noon, dusk, and midnight sectors. MLT = magnetic local time.

amount of the dependence on high solar wind ram pressure is more subtle. There is only a small percentage where high pressure has been important.

Figure 20 shows the solar wind ram pressure during the high intensity plasmaspheric hiss intervals for the (a) dawn sector, (b) the noon sector, (c) the dusk sector, and (d) the midnight sector. The plasmaspheric hiss is shown in the white/gray bars in normalized percent occurrence, and the annual ram pressure percent occurrences is shown in black bars.

The important result from this figure is that the intense plasmaspheric hiss part of the time occurs during high solar wind ram pressure intervals for both the noon sector and the midnight sector. The results for the noon sector are expected from Falkowski et al. (2017). See the scenario in the discussion of Figure 18. The midnight sector result, although somewhat surprising is supportive of the high SYM-H* value dependence found for the waves in Figure 18d.

The local time sector is the dusk sector, Figure 18d. Almost all events occurred when the solar wind ram pressure was less than 2 nPa.

4. Summary

The following are the main findings of our study of intense plasmaspheric hiss:

1. Using 1 year of ~300-Hz to ~1-kHz plasmaspheric hiss events (April 1996 to April 1997), detailed minimum variance analyses were performed on the 10 most intense plasmaspheric hiss event intervals (satellite tracks) for four MLT sectors (midnight, dawn, noon, and dusk). The most important result of this study is that plasmaspheric hiss was found to be coherent in all 40 event intervals. This will have important consequences for particle precipitation through coherent wave-particle interactions.

2. It was found that plasmaspheric hiss can be circularly, elliptically, and linearly polarized (Figures 4–9). There is no particular dependence on MLT or L for the elliptical and linearly polarized plasmaspheric hiss. Studying the 200 individual wave cycles, no strong θ_{kB} dependence on either L or MLAT was found (Figure 12). However, having stated that there is a slight dependence for low θ_{kB} (<40°) values to occur close to the magnetic equator and higher θ_{kB} values to be at larger |MLAT|. Most waves were determined to be elliptically polarized (Figure 13). Elliptical polarizations were detected for all θ_{kB} from 0° to 90°. Circular polarizations were also detected for all θ_{kB} but with less frequency than for elliptical

polarizations. Linearly polarized waves were detected only for $\theta_{kB} \geq 50°$. It should be noted that the magnetic component elliptical hiss is expected for the high plasma density plasmasphere, whereas the low density outer magnetospheric chorus is always (magnetically) circularly polarized (Verkhoglyadova et al., 2010).

3. The intensities of the selected plasmaspheric hiss wave event intervals display no obvious latitudinal |MLAT| dependences (Figure 11). The waves are equally intense at 50° to 60° |MLAT| as at the magnetic equator.

4. The intense wave percent occurrence dependences on AE* was determined (Figures 15 and 16). It was found that the dawn and noon waves were strongly substorm (AE*) dependent. There was a lack of AE* dependence in the dusk sector.

5. The same study as summarized in item 4 was done for SYM-H* (Figures 17 and 18). It was found that the local time sector with the largest negative SYM-H* dependence was noon. This is consistent with the substorm AE* dependence mentioned above and the results of prior studies. The midnight sector showed a positive SYM-H* plasmaspheric hiss dependence. This is unexpected and needs physical explanation.

6. The solar wind ram pressure was studied for the intense plasmaspheric hiss event interval data. No time delays were assumed. Solar wind ram pressure dependences on the waves were found in the noon sector and the midnight sector. The noon sector result is consistent with the previous Falkowski et al. (2017) result. The midnight sector result is consistent with the SYM-H* result mentioned in item 5.

7. Statistical analyses indicated that plasmaspheric hiss occurs most frequently on the duskside of the plasmasphere (Figure 1). A similar result for a different frequency range of plasmaspheric hiss was previously shown in Tsurutani et al. (2015). A slightly different statistical survey indicated that the waves are most intense (by an order of magnitude in nT^2/Hz) on the dayside (Figure 2). This result is the same as the Meredith et al. (2004) result.

5. Discussion and Conclusions

Ten of the most intense ~2 min of plasmaspheric hiss data were selected from each of the four local time sectors. All 40 of the events contained many coherent approximately three to five cycles of coherent waves. This implies that the presence of high intensity, coherent plasmaspheric hiss at all local times should dominate wave-particle interactions in the plasmasphere. It was previously shown that coherent wave-particle interactions will be approximately three orders of magnitude faster than incoherent wave-particle interactions (Bellan, 2013; Lakhina et al., 2010). It is our thought that coherence is thus perhaps a more important property than wave intensity for wave-particle interaction calculations concerning plasmaspheric hiss. One possibility of this result is that the L = 2 to 3 energetic electron slot/trough is formed by cyclotron interaction with these coherent waves. These interactions will take place not only at local noon but at all local times.

The plasmaspheric hiss waves were found to be not only circularly polarized but also elliptically and linearly polarized as well. There was no obvious dependence of the elliptically and linearly polarized waves on plasmaspheric location such as L and MLAT. The waves were equally intense at 50° to 60° MLAT as at the magnetic equator. The wave intensities were statistically nearly the same at all |MLAT| values.

It should be mentioned that the obliquely propagating plasmaspheric hiss may have other consequences for the precipitation for electrons in and near the slot region. Artemyev et al. (2013, 2015, 2016) have argued that energetic electron interaction with obliquely propagating electromagnetic waves could lead to further particle energy gain. This might be particularly true in the plasmasphere where large amplitude oblique waves are present everywhere in the plasmasphere with comparable intensities both in the equatorial plane and at high MLATs. It also should be noted that inner zone plasmaspheric hiss is exceptionally intense during magnetic storms (Smith et al., 1974; Tsurutani et al., 1975). Comparison of the equatorial electron spectrum to the precipitating spectrum could assess how big of a factor this mechanism is.

How can one interpret the above findings? If it is outer zone chorus that is the source for the intense and coherent plasmaspheric hiss, it should first be noted that the ~0.1- to 0.5-s chorus elements are composed of many coherent, monochromatic subelements composed of ~3 to ~10 wave cycles (Lakhina et al., 2010; Tsurutani et al., 2009; Tsurutani, Falkowski, et al., 2011). For rising tone chorus elements, all of the
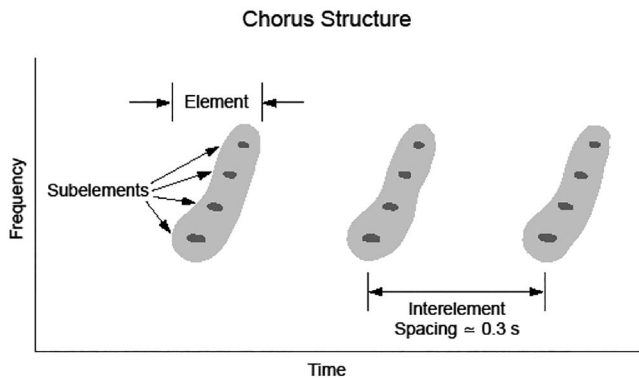
Figure 21. Chorus rising tone *elements* and monochromatic *subelements*. Each element is composed of many monochromatic subelements, the next being at a higher frequency than the previous subelement. This sequence of higher frequency subelements within an element gives the rising tone (increase in frequency) appearance of the chorus element.

subelements will occur at different frequencies (shown in Figure 21). This is our idea of what a chorus rising element looks like in high resolution.

Figure 22 shows a schematic of how each subelement, starting at the magnetic equator with the same parallel propagating ($\theta_{kB} = 0$) wave direction, propagates into the plasmasphere. Three subelements are depicted with ~0.1, 0.2, and 0.3 fce, where fce is the electron cyclotron frequency. The entry of the subelements into the plasmasphere will occur at different physical locations of the plasmapause. The subsequent subelement wave refraction inside the plasmasphere will be different as well. Thus, one possible picture is that all of the monochromatic subelements originating at different L in the outer magnetosphere will be populating the inner plasmasphere at different MLATs, giving this observational result of small intervals of wave coherence.

The presence of obliquely propagating waves with a variety of polarizations (circular, elliptical, and linear) will have strong effects on wave-particle interactions. It is clear that models using parallel propagating, circularly polarized waves will only be a first step in computer modeling efforts.

The fact that the waves are intense at all magnetic latitudes can be explained by this picture of the entry of many, many small subelement approximately three- to five-cycle coherent wave packets. This should be simpler for modeling purposes. It is noted that this result is different than the recent Meredith et al. (2018) finding of two distinct bands, one near the equator and a second one at higher magnetic latitudes. However, the reader should note that the present result is not inconsistent with that of Meredith et al. (2018). Here only the most intense plasmaspheric hiss has been studied.

Plasmaspheric hiss intense event interval data were examined for AE* (substorm) dependences. For AE*, there was a clear high AE* value distribution for the dawn and noon sectors. This is consistent with intense plasmaspheric hiss being related to substorms (HILDCAAs) and chorus generation, a result in good agreement with Meredith et al. (2018). Energetic ~10- to 100-keV anisotropic electron injection in the midnight sector during substorms with subsequent drift to the noon sector will result in chorus generation during these sectors. Subsequent chorus subelement propagation into the plasmasphere can explain the observations presented here.

Plasmaspheric hiss intense event interval data were also examined for SYM-H* and solar wind ram pressure dependences (Figures 17–20). The SYM-H* results were similar to that for AE* for the dawn and noon local time sectors. The results are consistent with outer zone chorus generation during substorm/HILDCAA intervals. The solar wind ram pressure results (with no time delays) confirm prior results indicating that local noon plasmaspheric hiss can also be associated with high solar wind pressures at times (Falkowski et al., 2017; Kim et al., 2015; Tsurutani et al., 2015). So the intense dayside plasmaspheric hiss has two origins, substorm gradient drifting outer zone ~10- to 100-keV electrons and also ram pressure betatron acceleration of remnant outer zone radiation belt electrons in minimum B pockets. From this study it appears as if the substorm source is the more important of the two.

A surprise is the midnight sector intense plasmaspheric hiss event intervals on positive SYM-H* values (no time delays are taken for this sector). The dependence of these waves on high solar wind ram pressures is confirmation of the positive SYM-H* results. It was also noted earlier that the midnight sector intense plasmaspheric hiss was AE* (again, no time delays were taken for this time sector) dependent. What could be the physical explanation for the above findings?

Another puzzling result is that although plasmaspheric hiss is detected most frequently in the dusk sector (Figure 1), intense plasmaspheric hiss is not substorm AE* dependent (Figure 16). Intense dusk sector
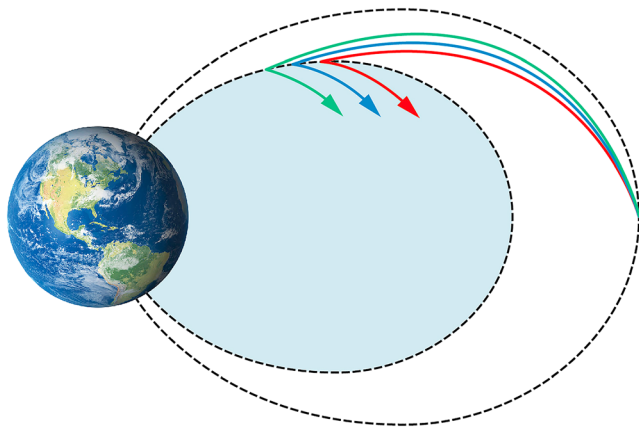
Figure 22. Three subelements of a chorus element propagating from their equatorial generation region to the plasmasphere (indicated in blue) and refracting into the high plasma density region.

plasmaspheric hiss occurs during slightly negative SYM-H* intervals (Figure 18). Dusk sector plasmaspheric hiss also occurs during low solar wind ram pressure intervals. One possible scenario explaining all of these dusk sector features is that the ring current recovery time scale for HILDCAA events is several hours or more in duration. Thus, although the SYM-H* value for a plasmaspheric hiss event is slightly negative, indicating prior ring current activity, it might be a remnant ring current that is being measured.

What is the source for the dusk sector plasmaspheric hiss? Our thought is it may be remnant substorm ~10–100-keV electrons drifting into a recovering (expanding) plasmaspheric bulge in the evening sector. This scenario was previously mentioned in Tsurutani et al. (2015) and still remains a possibility. How would such waves be generated? It could be the Thorne et al. (1979) mechanism of circulation of local plasmaspheric hiss with multiple passages through the generation region. However, it should be mentioned that the waves in this local time sector look essentially the same as in other local time sectors (not shown for brevity). Another piece of information is that hiss is detected outside the nominal L = 6 to 8 location of the plasmapause (Summers et al., 2008; Tsurutani et al., 2015). These *hiss fingers* are most likely associated with hiss inside plasmaspheric plumes/tails. For waves to be generated as ~10- to 100-keV electrons gradient drift through such small spatial regions of high density plasma indicates possible evidence of much more rapid wave growth. Thus, we suggest that theoretical plasma physicists try to employ nonlinear wave growth formalisms to determine if both dusk sector intense plasmaspheric hiss and plasmaspheric tail hiss can be generated locally.

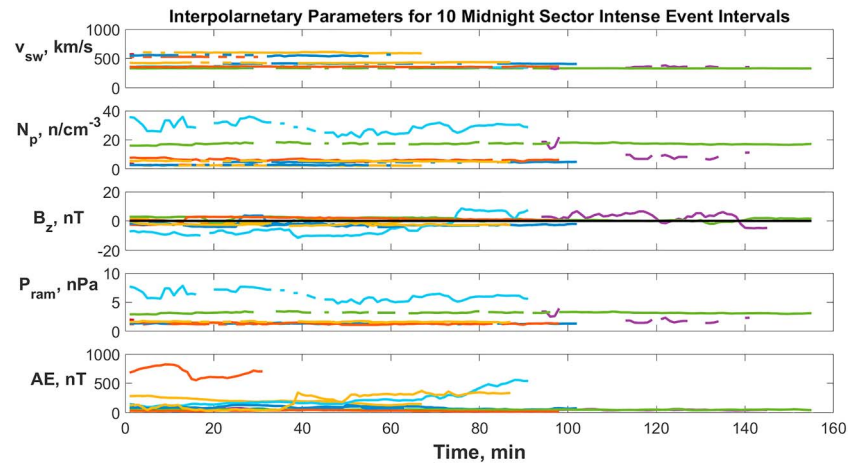### 5.1. Midnight Sector Intense, Coherent Waves

Because intense, coherent plasmaspheric hiss was detected in the midnight sector, we looked into this further with hopes of understanding the seemingly anomalous results of both high and low solar wind ram pressures and high and low AE values. To look at things in a different way, the solar wind data were plotted (without time delays) for all 10 event intervals. This is shown in Figure 23.

The solar wind data for the 10 midnight sector intense event wave intervals are given in Figure 23. From top to bottom are the solar wind velocity, density, IMF Bz, solar wind ram pressure, and the AE index. No time delays were used for any of the above parameters (other than the normal solar wind propagation from the spacecraft to the Earth's bow shock). What is quite apparent is that there are a couple of outlier events. Two of them have high solar wind speeds (>500 km/s), densities, and thus high ram pressures (first, second, and fourth bottom panels, respectively). There is one event with large negative IMF Bz (third panel) and correspondingly high AE (bottom panel). This is the same event. If one looks around these outlying events, the typical solar wind speed is Vsw < 400 km/s, density is <5 cm^{-3}, ram pressure < 2 nPa, and AE < 200 nT. These properties are those of a quiet solar wind and also a geomagnetically quiet magnetosphere.

One possible suggestion is that these are not substorm-generated midnight sector chorus waves which have propagated into the plasmasphere. There seems to be little or no evidence for this argument. If this is correct, then what is the source of intense plasmaspheric hiss in this local time sector? One possibility is that these waves enter the plasmasphere in a different local time sector and then propagate to the midnight sector (L. Chen et al., 2009). Another possibility is that during high solar wind ram pressure events, the distortion of the nightside magnetospheric magnetic fields readily allow chorus penetration into the plasmasphere. Further studies will be needed on this topic to see which scenario is the correct one or if there is some other more plausible explanation.

5.2. Final Comments

The main purpose of this paper was to show that plasmaspheric hiss is coherent, contrary to many published statements in the past. The coherency occurs in bunches of approximately three- to five-wave cycles. Besides showing a few examples of five-wave cycles, we have shown large stretches (~0.4 s) of waves so that the reader can see that these *subelements* exist everywhere. This was our general finding for all of the 40 plasma hiss wave event intervals studied. A nonwave person might say, "just a bunch of wiggles in the magnetic (and electric) fields, so what?" Coherent (and incoherent) waves have strong effects on the losses of energetic electrons. For example, Horne and Thorne (1998) suggested that outer zone chorus could parasitically interact with relativistic electrons at off-axis locations (large MLATs) and cause pitch angle scattering and loss to the ionosphere as ~0.1- to 0.5-s *relativistic microbursts*. However, with the discovery that chorus subelements were coherent in the equatorial plane generation region, but not at off-axis locations

Figure 23. Solar wind and AE data for the midnight sector event intervals. The different colors correspond to the 10 midnight sector intense plasmaspheric hiss intervals.

(Tsurutani et al., 2009, 2013; Tsurutani, Falkowski, et al., 2011), the latter authors questioned the existence of relativistic microbursts (unless there were plasma ducts guiding the chorus). It was shown that coherent electromagnetic ion cyclotron waves could easily cause the loss of relativistic $E > 1$–2-MeV electrons in the outer $L > 6$ magnetosphere during solar wind pressure pulses and fast forward shocks (Hajra & Tsurutani, 2017; Remya et al., 2015; Tsurutani et al., 2016).

Coherent plasmaspheric hiss could be the phenomenon that causes the loss of relativistic electrons in the inner ($L < 6$) magnetosphere. Because of the high plasma densities inside the plasmasphere, the electromagnetic wave phase speed will be substantially smaller than in the low-density outer magnetosphere. The local magnetic field will be considerably higher at these distances closer to Earth. Both factors will lead to higher cyclotron resonant energies of electrons. The finding that intense plasmaspheric hiss is present at all magnetic latitudes indicates that the electrons will cyclotron resonate with multiple subelement wave packets during a bounce period. Calculations of the details of relativistic electron precipitation in the inner magnetosphere are beyond the scope of the present paper, but we encourage others to attempt to do this.

References

Agapitov, O., Artemyev, A., Krasnoselskikh, V., Khotyaintsev, Y. V., Mourenas, D., Breuillard, H., et al. (2013). Statistics of whistler mode waves in the outer radiation belt: Cluster STAFF-SA measurements. *Journal of Geophysical Research: Space Physics*, *118*, 3407–3420. https://doi.org/10.1002/jgra.50312

Agapitov, O. V., Artemyev, A. V., Mourenas, D., Kasahara, Y., & Krasnoselskikh, V. (2014). Inner belt and slot region electron lifetimes and energization rates based on Akebono statistics of whistler waves. *Journal of Geophysical Research: Space Physics*, *119*, 2876–2893. https://doi.org/10.1002/2014JA019886

Artemyev, A., Agapitov, O., Mourenas, D., Krasnoselskikh, V., Shastun, V., & Mozer, F. (2016). Oblique whistler-mode waves in the Earth's inner magnetosphere: Energy distribution, origins, and role in radiation belt dynamics. *Space Science Reviews*, *200*(1–4), 261–355. https://doi.org/10.1007/s11214-016-0252-5

Artemyev, A. V., Agapitov, O. V., Mourenas, D., Krasnoselskikh, V., & Zelenyi, L. M. (2013). Storm-induced energization of radiation belt electrons: Effect of wave obliquity. *Geophysical Research Letters*, *40*, 4138–4143. https://doi.org/10.1002/grl.50837

Artemyev, A. V., Agapitov, O. V., Mourenas, D., Krasnoselskikh, V. V., & Mozer, F. S. (2015). Wave energy budget analysis in the Earth's radiation belts uncovers a missing energy. *Nature Communications*, *6*(1). https://doi.org/10.1038/ncomms8143

Bellan, P. M. (2013). Pitch angle scattering of an energetic magnetic particle by a circularly polarized electromagnetic wave. *Physics of Plasmas*, *20*, 042117. https://doi.org/10.1063/1.4801055

Bortnik, J., Chen, L., Li, W., Thorne, R. M., Meredith, N. P., & Horne, R. B. (2011). Modeling the wave power distribution and characteristics of plasmaspheric hiss. *Journal of Geophysical Research*, *116*, A12209. https://doi.org/10.1029/2011JA016862

Bortnik, J., Li, W., Thorne, R. M., Angelopoulos, V., Cully, C., Bonnell, J., et al. (2009). An observation linking the origin of plasmaspheric hiss to discrete chorus emissions. *Science*, *324*(5928), 775–778. https://doi.org/10.1126/science.1171273

Bortnik, J., Thorne, R. M., & Meredith, N. P. (2008). The unexpected origin of plasmaspheric hiss from discrete chorus emissions. *Nature*, *452*(7183), 62–66. https://doi.org/10.1038/nature06741

Bortnik, J., Thorne, R. M., & Meredith, N. P. (2009). Plasmaspheric hiss overview and relation to chorus. *Journal of Atmospheric and Solar - Terrestrial Physics*, *71*, 1636.

Breneman, A. W., Kletzing, C. A., Pickett, J., Chum, J., & Santolik, O. (2009). Statistics of multispacecraft observations of chorus dispersion and source location. *Journal of Geophysical Research*, *114*, A06202. https://doi.org/10.1029/2008JA013549

Carpenter, D. L. (1978). New whistler evidence of a dynamo origin of electric fields in the quiet plasma. *Journal of Geophysical Research*, *83*, 44.

Chen, A. J., & Grebowsky, J. M. (1974). Plasma tail interpretations of pronounced detached plasma regions measured by OGO 5. *Journal of Geophysical Research*, *79*(25), 3851–3855. https://doi.org/10.1029/JA079i025p03851

Chen, L., Bortnik, J., Li, W., Thorne, R. M., & Horne, R. B. (2012). Modeling the properties of plasmaspheric hiss: 1. Dependence on chorus wave emission. *Journal of Geophysical Research*, *117*, A05201. https://doi.org/10.1029/2011JA017201

Chen, L., Bortnik, J., Thorne, R. M., Horne, R. B., & Jordanova, V. K. (2009). Three-dimensional ray tracing of VLF waves in a magnetospheric environment containing a plasma plume. *Geophysical Research Letters*, *36*, L22101. https://doi.org/10.1029/2009GL040451

Chen, L., Thorne, R. M., Bortnik, J., Li, W., Horne, R. B., Reeves, G. D., et al. (2014). Generation of unusually low frequency plasmaspheric hiss. *Geophysical Research Letters*, *41*, 5702–5709. https://doi.org/10.1002/2014GL060628

Cornilleau-Wehrlin, N., Gendrin, R., Lefeuvre, F., Parrot, M., Grard, R., Jones, D., et al. (1978). VLF electromagnetic waves observed onboard GEOS-1. *Space Science Reviews*, *22*, 371.

Cornilleau-Wehrlin, N., Solomon, J., Korth, A., & Kremser, G. (1993). Generation mechanism of plasmaspheric ELF/VLF hiss: A statistical study from GEOS 1 data. *Journal of Geophysical Research*, *98*(A12), 21,471–21,479. https://doi.org/10.1029/93JA01919

Delport, B., Collier, A. B., Lichtenberger, J., Rodger, C. J., Parrot, M., Clilverd, M. A., & Friedel, R. H. W. (2012). Simultaneous observation of chorus and hiss near the plasmapause. *Journal of Geophysical Research*, *117*, A12218. https://doi.org/10.1029/2012JA017609

Falkowski, B. J., Tsurutani, B. T., Lakhina, G. S., & Pickett, J. S. (2017). Two sources of dayside intense, quasi-coherent plasmaspheric hiss: A new mechanism for the slot region? *Journal of Geophysical Research: Space Physics*, *122*, 1643–1657. https://doi.org/10.1002/2016JA023289

Gail, W. B., & Inan, U. S. (1990). Characteristics of wave-particle interactions during sudden commencements: 2. Spacecraft observations. *Journal of Geophysical Research*, *95*(A1), 139–147. https://doi.org/10.1029/JA095iA01p00139

Gail, W. B., Inan, U. S., Helliwell, R. A., Carpenter, D. L., Krisnaswamy, S., Rosenberg, T. J., & Lanzerotti, L. J. (1990). Characteristics of wave-particle interactions during sudden commencements: 1. Ground-based observations. *Journal of Geophysical Research*, *95*(A1), 119–137. https://doi.org/10.1029/JA095iA01p00119

Gao, Y., Xiao, F., Yan, Q., Yang, C., Liu, S., He, Y., & Zhou, Q. (2015). Influence of wave normal angles on hiss-electron interactions in Earth's slot region. *Journal of Geophysical Research: Space Physics*, *120*, 9385–9400. https://doi.org/10.1002/2015JA021786

Glauert, S. A., Horne, R. B., & Meredith, N. P. (2014). Three-dimensional electron radiation belt simulations using the BAS radiation belt model with new diffusion models for chorus, plasmaspheric hiss and lightning-generated whistlers. *Journal of Geophysical Research: Space Physics*, *119*, 268–289. https://doi.org/10.1002/2013JA019281

Golden, D. I., Spasojevic, M., Li, W., & Nishimura, Y. (2012). Statistical modeling of plasmaspheric hiss amplitude using solar wind measurements and geomagnetic indices. *Geophysical Research Letters*, *39*, L06103. https://doi.org/10.1029/2012GL051185

Gonzalez, W. D., Joselyn, J. A., Kamide, Y., Kroehl, H. W., Rostoker, G., Tsurutani, B. T., & Vasyliunas, V. M. (1994). What is a geomagnetic storm? *Journal of Geophysical Research*, *99*(A4), 5771–5792. https://doi.org/10.1029/93JA02867

Green, J. L., Boardsen, S., Garcia, L., Taylor, W. W. L., Fung, S. F., & Reinisch, B. W. (2005). On the origin of whistler mode radiation in the plasmasphere. *Journal of Geophysical Research*, *110*, A03201. https://doi.org/10.1029/2004JA010495

Gurnett, D. A., Persoon, A. M., Randall, R. F., Odem, D. L., Remington, S. L., Averkamp, T. F., et al. (1995). The Polar plasma wave instrument. *Space Science Reviews*, *71*(1-4), 597–622. https://doi.org/10.1007/BF00751343

Hajra, R., Echer, E., Tsurutani, B. T., & Gonzalez, W. D. (2013). Solar cycle dependence of High-Intensity Long-Duration Continuous AE Activity (HILDCAA) events, relativistic electron predictors? *Journal of Geophysical Research: Space Physics*, *118*, 5626–5638. https://doi.org/10.1002/jgra.50530

Hajra, R., Echer, E., Tsurutani, B. T., & Gonzalez, W. D. (2014). Superposed epoch analyses of HILDCAAs and their interplanetary drivers: Solar cycle and seasonal dependences. *Journal of Atmospheric and Solar - Terrestrial Physics*, *121*, 24–31. https://doi.org/10.1016/j.jastp.2014.09.012

Hajra, R., & Tsurutani, B. T. (2017). Magnetospheric "killer" relativistic electron dropouts (REDs) and repopulation: A cyclical process. In N. Buzulukova (Ed.), *Extreme events in geospace* (Chap 14, pp. 374–391). Cambridge, MA: Elsevier. https://doi.org/10.1016/B978-0-12-812700-1.00014-5

Hayakawa, M., & Sazhin, S. S. (1992). Mid-latitude and plasmaspheric HISS-A review. *Planetary and Space Science*, *40*(10), 1325–1338. https://doi.org/10.1016/0032-0633(92)90089-7

Horne, R. B., & Thorne, R. M. (1998). Potential waves for relativistic electron scattering and stochastic acceleration during magnetic storms. *Geophysical Research Letters*, *25*(15), 3011–3014. https://doi.org/10.1029/98GL01002

Horne, R. B., Wheeler, G. V., St, H., & Alleyne, C. K. (2000). Proton and electron heating by radially propagating fast magnetosonic waves. *Journal of Geophysical Research*, *105*(A12), 27,597–27,610. https://doi.org/10.1029/2000JA000018

Kim, K.-C., Lee, D.-Y., & Shprits, Y. (2015). Dependence of plasmaspheric hiss on solar wind parameters and geomagnetic activity and modeling of its global distribution. *Journal of Geophysical Research: Space Physics*, *120*, 1153–1167. https://doi.org/10.1002/2014JA020687

Kokubun, S. (1983). Characteristics of storm sudden commencements at geostationary orbit. *Journal of Geophysical Research*, *88*(A12), 10025. https://doi.org/10.1029/JA088iA12p10025

Korth, A., Kremser, G., Cornilleau-Wehrlin, N., & Solomon, J. (1986). Observations of energetic electrons and VLF waves at geostationary orbit during storm sudden commencements (SSC). In Y. Kamide & J. A. Slavin (Eds.), *Sol. Wind-Magn. Coupling* (Vol. 391, pp. 391–399). Tokyo: Terra Sci. Publ.

Lakhina, G. S., Tsurutani, B. T., Verkhoglyadova, O. P., & Pickett, J. S. (2010). Pitch angle transport of electrons due to cyclotron interactions with coherent chorus subelements. *Journal of Geophysical Research*, *117*, A00F15. https://doi.org/10.1029/2009JA014885

Li, W., Chen, L., Bortnik, J., Thorne, R. M., Angelopoulos, V., Kletzing, C. A., et al. (2015). First evidence for chorus at a large geocentric distance as a source of plasmaspheric hiss: Coordinated THEMIS and Van Allen Probes observation. *Geophysical Research Letters*, *42*, 241–248. https://doi.org/10.1002/2014GL062832

Li, W., Chen, L., Bortnik, J., Thorne, R. M., Angelopoulos, V., Kletzing, C. A., et al. (2017). First evidence for chorus at a large geocentric distance as a source of plasmaspheric hiss: Coordinated THEMIS and Van Allen Probes observation. *Geophysical Research Letters*, *42*, 241–248. https://doi.org/10.1002/2014GL062832

Li, W., Ma, Q., Thorne, R. M., Bortnik, J., Kletzing, C. A., Kurth, W. S., et al. (2015). Statistical properties of plasmaspheric hiss derived from Van Allen Probes data and their effects on radiation belt electron dynamics. *Journal of Geophysical Research: Space Physics*, *120*, 3393–3405. https://doi.org/10.1002/2015JA021048

Li, W., Mourenas, D., Artemyev, A. V., Agapitov, O. V., Bortnik, J., Albert, J. M., et al. (2014). Evidence of stronger pitch angle scattering loss caused by oblique whistler-mode waves as compared with quasi-parallel waves. *Geophysical Research Letters*, *41*, 6063–6070. https://doi.org/10.1002/2014GL061260

Li, W., Thorne, R. M., Bortnik, J., Reeves, G. D., Kletzing, C. A., Kurth, W. S., et al. (2013). An unusual enhancement of low-frequency plasmaspheric hiss in the outer plasmasphere associated with substorm-injected electrons. *Geophysical Research Letters*, *40*, 3798–3803. https://doi.org/10.1002/grl.50787

Liu, N., Su, Z., Gao, Z., Zheng, H., Wang, Y., Wang, S., et al. (2017). Simultaneous disappearances of plasmaspheric hiss, exohiss and chorus waves triggered by a sudden decrease in solar wind dynamic pressure. *Geophysical Research Letters*, *44*, 52–61. https://doi.org/10.1002/2016GL071987

Malaspina, D. M., Jaynes, A. N., Boule, C., Bortnik, J., Thaller, S. A., Ergun, R. E., et al. (2016). The distribution of plasmaspheric hiss wave power with respect to the plasmapause location. *Geophysical Research Letters*, *43*, 7878–7886. https://doi.org/10.1002/2016GL069982, doi:10.1002/2016GL069982

Malaspina, D. M., Jaynes, A. N., Hospodarsky, G., Bortnik, J., Ergun, R. E., & Wygant, J. (2017). Statistical properties of low-frequency plasmaspheric hiss. *Journal of Geophysical Research: Space Physics*, *122*, 8340–8352. https://doi.org/10.1002/2017JA024328

Meredith, N. P., Horne, R. B., & Anderson, R. R. (2001). Substorm dependence of chorus amplitudes: Implications for the acceleration of electrons to relativistic energies. *Journal of Geophysical Research*, *106*(A7), 13,165–13,178. https://doi.org/10.1029/2000JA900156

Meredith, N. P., Horne, R. B., Clilverd, M. A., Horsfall, D., Thorne, R. M., & Anderson, R. R. (2006). Origins of plasmaspheric hiss. *Journal of Geophysical Research*, *111*, A09217. https://doi.org/10.1029/2006JA011707

Meredith, N. P., Horne, R. B., Glauert, S. A., & Anderson, R. R. (2007). Slot region electron loss timescales due to plasmaspheric hiss and lightning-generated whistlers. *Journal of Geophysical Research*, *112*, A08214. https://doi.org/10.1029/2007JA012413

Meredith, N. P., Horne, R. B., Kersten, T., Li, W., Bortnik, J., Sicard, A., & Yearby, K. H. (2018). Global model of plasmaspheric hiss from multiple satellite observations. *Journal of Geophysical Research: Space Physics*, *123*, 4526–4541. https://doi.org/10.1029/2018JA025226

Meredith, N. P., Horne, R. B., Sicard-Piet, A., Boscher, D., Yearby, H., Li, W., & Thorne, R. M. (2012). Global model of lower band and upper band chorus from multiple satellite observations. *Journal of Geophysical Research*, *117*, A10225. https://doi.org/10.1029/2012JA017978

Meredith, N. P., Horne, R. B., Thorne, R. M., Summers, D., & Anderson, R. R. (2004). Substorm dependence of plasmaspheric hiss. *Journal of Geophysical Research*, *109*, A06209. https://doi.org/10.1029/2004JA010387

Orlova, K., Spasojevic, M., & Shprits, Y. (2014). Activity-dependent global model of electron loss inside the plasmasphere. *Geophysical Research Letters*, *41*, 3744–3751. https://doi.org/10.1002/2014GL060100

Parrot, M., Santolik, O., Gurnett, D., Pickett, J., & Cornilleau-Wehrlin, N. (2004). Characteristics of magnetospherically reflected chorus waves observed by Cluster. *Annales de Geophysique*, *22*(7), 2597–2606. https://doi.org/10.5194/angeo-22-2597-2004

Perraut, S., Roux, A., Robert, P., Gendrin, R., Sauvaud, J.-A., Bosqued, J.-M., et al. (1982). A systematic study of ULF waves above F_{H+} from GEOS 1 and 2 measurements and their relationships with proton ring distributions. *Journal of Geophysical Research*, *87*(A8), 6219–6236. https://doi.org/10.1029/JA087iA08p06219

Remya, B., Tsurutani, B. T., Reddy, R. V., Lakhina, G. S., & Hajra, R. (2015). Electromagnetic cyclotron waves in the dayside subsolar outer magnetosphere generated by enhanced solar wind pressure: EMIC wave coherency (2015). *Journal of Geophysical Research: Space Physics*, *120*, 7536–7551. https://doi.org/10.1002/2015JA021327

Santolik, O. (2008). New results of investigations of whistler-mode chorus emissions. *Nonlinear Processes in Geophysics*, *15*(4), 621–630. https://doi.org/10.5194/npg-15-621-2008

Santolik, O., & Chum, J. (2009). The origin of plasmaspheric hiss. *Science*, *324*(5928), 729–730. https://doi.org/10.1126/science.1172878

Santolik, O., Chum, J., Parrot, M., Gurnett, D. A., Pickett, J. S., & Cornilleau-Wehrlin, N. (2006). Propagation of whistler mode chorus to low altitudes: Spacecraft observations of structured ELF hiss. *Journal of Geophysical Research*, *111*, A10208. https://doi.org/10.1029/2005JA011462

Santolik, O., Parrot, M., Storey, L. R. O., Pickett, J. S., & Gurnett, D. A. (2001). Propagation analysis of plasmaspheric hiss using Polar PWI measurements. *Geophysical Research Letters*, *28*(6), 1127–1130. https://doi.org/10.1029/2000GL012239

Santolik, O., Pickett, J. S., Gurnett, D. A., Maksimovic, M., & Cornilleau-Wehrlin, N. (2002). Spatiotemporal variability and propagation of equatorial noise observed by Cluster. *Journal of Geophysical Research*, *107*(A12), 1495. https://doi.org/10.1029/2001JA009159

Shinbori, A., Ono, T., Iizima, M., & Kumamoto, A. (2003). Sudden commencements related plasma waves observed by the Akebono satellite in the polar region and inside the plasmasphere region. *Journal of Geophysical Research*, *108*(A12), 1457. https://doi.org/10.1029/2003JA009964

Smith, E. J., Frandsen, A. M. A., Tsurutani, B. T., Thorne, R. M., & Chan, K. W. (1974). Plasmasheric hiss intensity variations during magnetic storms. *Journal of Geophysical Research*, *79*(16), 2507–2510. https://doi.org/10.1029/JA079i016p02507

Smith, E. J., & Tsurutani, B. T. (1976). Magnetosheath lion roars. *Journal of Geophysical Research*, *81*(13), 2261–2266. https://doi.org/10.1029/JA081i013p02261

Smith, E. J., & Wolfe, J. H. (1976). Observations of interaction regions and corotating shocks between one and five AU: Pioneers 10 and 11. *Geophysical Research Letters*, *3*(3), 137–140. https://doi.org/10.1029/GL003i003p00137

Solomon, J., Cornilleau-Wehrlin, N., Korth, A., & Kremser, G. (1988). An experimental study of ELF/VLF hiss generation in the Earth's magnetosphere. *Journal of Geophysical Research*, *93*(A3), 1839. https://doi.org/10.1029/JA093iA03p01839

Spasojevic, M., Shprits, Y. Y., & Orlova, K. (2015). Global empirical models of plasmaspheric hiss using Van Allen probes. *Journal of Geophysical Research: Space Physics*, *120*, 10,370–10,383. https://doi.org/10.1002/2015JA021803

Storey, L. R. O., Lefeuvre, F., Parrot, M., Cairo, L., & Anderson, R. R. (1991). Initial survey of the wave distribution functions for plasmaspheric hiss observed by ISEE-1. *Journal of Geophysical Research*, *96*(A11), 19469. https://doi.org/10.1029/91JA01828

Su, Z., Zhu, H., Xiao, F., Zheng, H., Wang, Y., Shen, C., et al. (2015). Disappearance of plasmaspheric hiss following interplanetary shock. *Geophysical Research Letters*, *42*, 3129–3140. https://doi.org/10.1002/2015GL063906

Summers, D., Ni, B., Meredith, N. P., Horne, R. B., Thorne, R. M., Moldwin, M. B., & Anderson, R. R. (2008). Electron scattering by whistler-mode ELF hiss in plasmaspheric plumes. *Journal of Geophysical Research*, *113*, A04219. https://doi.org/10.1029/2007JA012678

Summers, D., Omura, Y., Nakamura, S., & Kletzing, C. A. (2014). Fine structure of plasmaspheric hiss. *Journal of Geophysical Research: Space Physics*, *119*, 9134–9149. https://doi.org/10.1002/2014JA020437

Thorne, R. M., Church, S. R., & Gorney, D. J. (1979). On the origin of plasmaspheric hiss: The importance of wave propagation during periods of substorm activity. *Journal of Geophysical Research*, *84*(A9), 5241. https://doi.org/10.1029/JA084iA09p05241

Thorne, R. M., Church, S. R., Malloy, W. J., & Tsurutani, B. T. (1977). The local time variation of ELF emissions during periods of substorm activity. *Journal of Geophysical Research*, *82*(10), 1585–1590. https://doi.org/10.1029/JA082i010p01585

Thorne, R. M., Smith, E. J., Burton, R. K., & Holzer, R. E. (1973). Plasmaspheric hiss. *Journal of Geophysical Research*, *78*(10), 1581–1596. https://doi.org/10.1029/JA078i010p01581

Thorne, R. M., Smith, E. J., Fiske, K. J., & Church, S. R. (1974). Intensity variation of ELF hiss and chorus during isolated substorms. *Geophysical Research Letters*, *1*(5), 193–196. https://doi.org/10.1029/GL001i005p00193

Tsurutani, B. T., Echer, E., & Gonzalez, W. D. (2011). The solar and interplanetary causes of the recent minimum in geomagnetic activity (MGA23): A combination of midlatitude small coronal holes, low IMF Bz variances, low solar wind speeds and low solar magnetic fields. *Annals of Geophysics*, *29*(1), 1–17. https://doi.org/10.5194/angeo-29-1-2011

Tsurutani, B. T., Falkowski, B. J., Pickett, J. S., Santolik, O., & Lakhina, G. S. (2015). Plasmaspheric hiss properties: Observations from Polar. *Journal of Geophysical Research: Space Physics*, *120*, 414–431. https://doi.org/10.1002/2014JA020518

Tsurutani, B. T., Falkowski, B. J., Pickett, J. S., Verkhoglyadova, O. P., Santolik, O., & Lakhina, G. S. (2014). Extremely intense ELF magnetosonic waves: A survey of Polar observations. *Journal of Geophysical Research: Space Physics*, *119*, 964–977. https://doi.org/10.1002/2013JA019284

Tsurutani, B. T., Falkowski, B. J., Verkhoglyadova, O. P., Pickett, J. S., Santolik, O., & Lakhina, G. S. (2011). Quasi-coherent chorus properties: 1. Implications for wave-particle interactions. *Journal of Geophysical Research*, *116*, A09210. https://doi.org/10.1029/2010JA016237

Tsurutani, B. T., Falkowski, B. J., Verkhoglyadova, O. P., Pickett, J. S., Santolik, O., & Lakhina, G. S. (2012). Dayside ELF electromagnetic wave survey: A Polar statistical study of chorus and hiss. *Journal of Geophysical Research*, *117*, A00L12. https://doi.org/10.1029/2011JA017180

Tsurutani, B. T., & Gonzalez, W. D. (1987). The cause of high-intensity long-duration continuous AE activity (HILDCAAS): Interplanetary Alfven wave trains. *Planetary and Space Science*, *35*(4), 405–412. https://doi.org/10.1016/0032-0633(87)90097-3

Tsurutani, B. T., Gonzalez, W. D., Gonzalez, A. L. C., Guarnieri, F. L., Gopalswamy, N., Grande, M., et al. (2006). Corotating solar wind streams and recurrent geomagnetic activity: A review. *Journal of Geophysical Research*, *111*, A07S01. https://doi.org/10.1029/2005JA011273

Tsurutani, B. T., Gonzalez, W. D., Gonzalez, A. L. C., Tang, F., Arballo, J. K., & Okada, M. (1995). Interplanetary origin of geomagnetic activity in the declining phase of the solar cycle. *Journal of Geophysical Research*, *100*(A11), 21,717–21,733. https://doi.org/10.1029/95JA01476

Tsurutani, B. T., Gonzalez, W. D., Guarnieri, F., Kamide, Y., Zhou, X.-Y., & Arballo, J. K. (2004). Are high-intensity, long-duration continuous AE activity (HILDCAA) events substorm expansion events? *Journal of Atmospheric and Solar - Terrestrial Physics*, *66*(2), 167–176. https://doi.org/10.1016/j.jastp.2003.08.015

Tsurutani, B. T., Hajra, R., Tanimori, T., Takada, A., Bhanu, R., Mannucci, A. J., et al. (2016). Heliospheric plasmasheet (HPS) impingement onto the magnetosphere as a cause of relativistic electron dropouts (REDs) via coherent EMIC wave scattering with possible consequences for climate change. *Journal of Geophysical Research: Space Physics*, *121*, 10,130–10,156. https://doi.org/10.1002/2016JA022499

Tsurutani, B. T., Lakhina, G. S., & Verkhoglyadova, O. P. (2013). Energetic electron (>10 keV) microburst precipitation, ~5–15s X-ray pulsations, chorus and wave-particle interactions: A review. *Journal of Geophysical Research: Space Physics*, *118*, 2296–2312. https://doi.org/10.1002/jgra.50264

Tsurutani, B. T., & Smith, E. J. (1974). Postmidnight chorus: A substorm phenomenon. *Journal of Geophysical Research*, *79*(1), 118–127. https://doi.org/10.1029/JA079i001p00118

Tsurutani, B. T., & Smith, E. J. (1977). Two types of magnetospheric ELF chorus and their substorm dependences. *Journal of Geophysical Research*, *82*(32), 5112–5128. https://doi.org/10.1029/JA082i032p05112

Tsurutani, B. T., Smith, E. J., & Thorne, R. M. (1975). Electromagnetic hiss and relativistic electron losses in the inner zone. *Journal of Geophysical Research*, *80*, 600.

Tsurutani, B. T., Verkhoglyadova, O. P., Lakhina, G. S., & Yagitani, S. (2009). Properties of dayside outer zone chorus during HILDCAA events: Loss of energetic electrons. *Journal of Geophysical Research*, *114*, A03207. https://doi.org/10.1029/2008JA013353

Verkhoglyadova, O. P., Tsurutani, B. T., & Lakhina, G. S. (2010). Properties of obliquely propagating chorus. *Journal of Geophysical Research*, *115*, A00F19. https://doi.org/10.1029/2009JA014809

Wang, C., Zong, Q., Xiao, F., Su, Z., Wang, Y., & Yue, C. (2011). The relations between magnetospheric chorus and hiss inside and outside the plasmasphere boundary layer: Cluster observation. *Journal of Geophysical Research*, *116*, A07221. https://doi.org/10.1029/2010JA016240

Yu, J., Li, L. Y., Cao, J. B., Chen, L., Wang, J., & Yang, J. (2017). Propagation characteristics of plasmaspheric hiss: Van Allen Probe observations and global empirical models. *Journal of Geophysical Research: Space Physics*, *122*, 4156–4167. https://doi.org/10.1002/2016JA023372

Yue, C., Chen, L., Bortnik, J., Ma, Q., Thorne, R. M., Angelopoulos, V., et al. (2017). The characteristic response of whistler mode waves to interplanetary shocks. *Journal of Geophysical Research: Space Physics*, *122*, 10,047–10,057. https://doi.org/10.1002/2017JA024574